

Virtual entanglement purification via noisy entanglement

Kaoru Yamamoto,^{1,*} Yuichiro Matsuzaki,² Yasunari Suzuki,¹ Yuuki Tokunaga,¹ and Suguru Endo^{1,3,†}

¹*NTT Computer and Data Science Laboratories, NTT Corporation, Musashino 180-8585, Japan*

²*Department of Electrical, Electronic, and Communication Engineering,
Faculty of Science and Engineering, Chuo University,*

1-13-27 Kasuga, Bunkyo-ku, Tokyo 112-8551, Japan

³*JST, PRESTO, 4-1-8 Honcho, Kawaguchi, Saitama, 332-0012, Japan*

Distributed quantum computation (DQC) is a promising approach for scalable quantum computing, where high-fidelity non-local operations among remote devices are required for universal quantum computation. These operations are typically implemented through state and gate teleportation with the consumption of high-fidelity entanglement prepared via entanglement purification. However, noisy local operations and classical communication (LOCC) limit the fidelity of purified entanglement, thereby degrading the quality of non-local operations. Meanwhile, circuit knitting and cutting, which simulate non-local operations by preparing separable states along with LOCC, has been considered for DQC as an alternative. Although this approach needs no entanglement among remote devices, it requires excessive circuit runs. Here, we present a protocol utilizing virtual operations that purifies noisy entanglement at the level of expectation values. Our protocol offers the following advantages over conventional methods: surpasses the fidelity limit of entanglement purification in the presence of noise in LOCC, requires fewer sampling shots than circuit knitting, and exhibits robustness against infidelity fluctuations in shared noisy Bell states, unlike probabilistic error cancellation. Our protocol bridges the gap between the entanglement-based and circuit-knitting DQC methods, offering a flexible approach to achieve further scalability despite hardware limitations.

Introduction.— Quantum computers promise to outperform classical computers in terms of computation power, but many physical qubits are essential for fault-tolerant computation. Although current technological advances have increased the number of qubits on a single quantum processing unit (QPU), greater scalability is crucial for achieving quantum supremacy. A promising approach for this scalability is distributed quantum computation (DQC) with a modular architecture, which requires high-fidelity entanglement generation and non-local operations among remote QPUs [1–17]. However, non-local operations realized in current experiments are still noisy [18–31]. Circuit knitting and cutting, which simulates non-local operations by preparing separable states along with local operations and classical communication (LOCC), has been considered for DQC as an alternative [32–36]. However, this approach requires excessive circuit runs, although it needs no entanglement.

A typical approach for realizing high-fidelity non-local operations is to utilize entanglement purification [37–45]: remote QPUs share noisy entanglement, generate high-fidelity entanglement from them by entanglement purification, and then consume the purified entanglement for state and gate teleportation via LOCC [46–50]. Entanglement purification is seen as promising for realizing high-fidelity non-local operations. However, the local noise in each QPU limits the maximally achievable fidelity of purified entanglement [41, 42]. For example, the order of 1% two-qubit gate error rate in a local QPU, which can be achieved in current integrated quantum computers [51], limits the minimum achievable infidelity to the order of 0.5% [41, 42]. This may not be sufficient for practical large-scale quantum computation with error correction. Researchers have investigated more efficient

protocols that can handle hardware limitations and imperfections [41–45].

To overcome this fidelity limitation, we leverage the concept of *virtual* operations, mainly developed within the field of quantum error mitigation (QEM) [52, 53]. Virtual operations mitigate errors at the level of expectation values by post-processing outputs from additional circuit runs in a classical manner rather than handling the quantum state itself. Here, we propose a virtual entanglement purification protocol via noisy-entanglement preparation by utilizing virtual operations confined to LOCC. Such virtually purified entanglement can be used for state and gate teleportation to realize high-fidelity non-local operations. Our demonstration shows, for noisy Bell states, significant advantages over conventional entanglement purification, circuit knitting, and probabilistic error cancellation (PEC) [54–56]. Our protocol produces purified Bell states with a leading-order infidelity term of $\frac{8}{15}p_2\epsilon$, where p_2 and ϵ are a local two-qubit gate error rate and the infidelity of initial noisy Bell states, respectively. Moreover, our protocol incurs much lower sampling overhead than circuit knitting by utilizing noisy entanglement as a resource: compared with the optimal circuit knitting, a noisy Bell state with 10% infidelity reduces the sampling overhead by around $(1/2)^n$ when simulating n purified Bell states. Finally, we demonstrate the robustness of our protocol against infidelity fluctuations in shared noisy Bell states unlike PEC [54–56], due to the error-agnostic property of our protocol. The proposed protocol bridges the gap between DQC with entanglement and that with circuit knitting, thus providing a flexible way for further scalability even with hardware limitations.

Virtual entanglement purification.— To explain

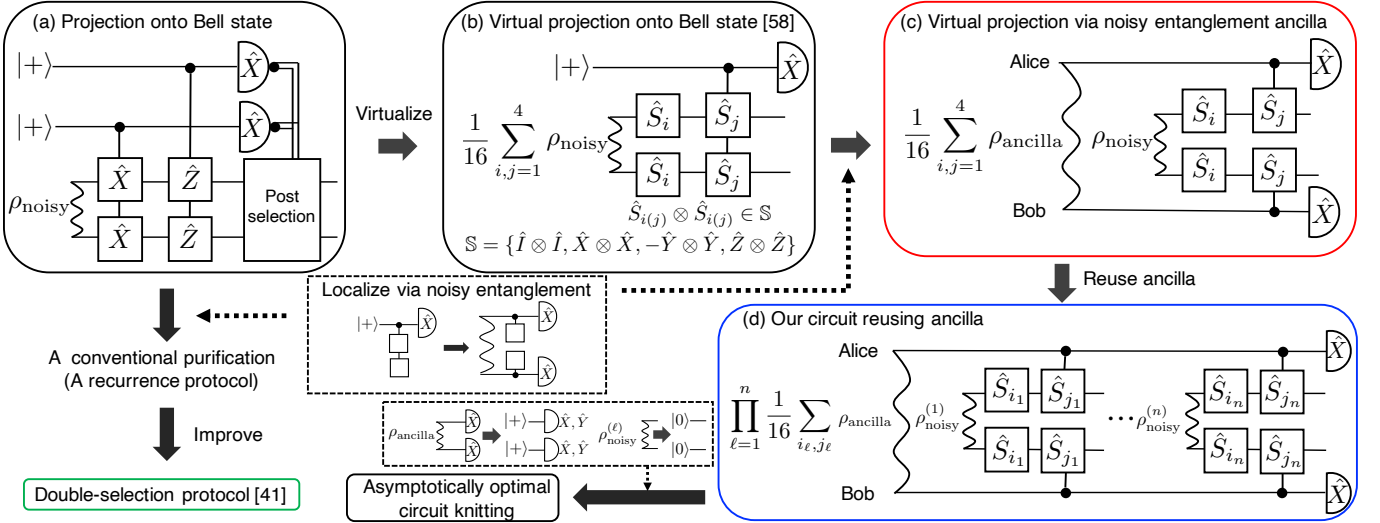


FIG. 1. Schematics of the overview and construction of our virtual circuit. (a) Purification with Bell-state projection by indirect measurement and post-selection, which is the origin of our virtual circuit as well as the conventional double-selection protocol [41]. (b) Virtual purification with Bell-state projection including non-local controlled operations. (c) Our virtual purification circuit with noisy-entanglement preparation and local-controlled operation. (d) Our circuit with ancilla reuse. Moreover, replacing all entanglement states with suitable separable states and additional measurements on the ancilla, shown here, provides the function of asymptotically optimal circuit knitting.

our quantum circuit, we start from the quantum circuit in Fig. 1(a). This circuit projects the input noisy state, ρ_{noisy} , onto the Bell state, $\rho_{\text{Bell}} = |\Psi_{\text{Bell}}\rangle\langle\Psi_{\text{Bell}}|$, $|\Psi_{\text{Bell}}\rangle = (|00\rangle + |11\rangle)/\sqrt{2}$, by indirectly measuring the stabilizer generators of the Bell states, $\hat{X} \otimes \hat{X}$ and $\hat{Z} \otimes \hat{Z}$, and then post-selecting the target state depending on the measurement results. This implements projection onto the Bell state, $\hat{P}_{\text{Bell}} = \left(\frac{\hat{I} \otimes \hat{I} + \hat{Z} \otimes \hat{Z}}{2}\right) \left(\frac{\hat{I} \otimes \hat{I} + \hat{X} \otimes \hat{X}}{2}\right)$ [57, 58]. Note that replacing the non-local controlled operations in Fig. 1(a) with noisy-entanglement preparation and local controlled operations, this circuit becomes a conventional purification circuit classified as a recurrence protocol, and its improved version is the double-selection protocol [41].

Tsubouchi *et al.* recently introduced virtual projection onto the stabilizer space [58]. Taking the projection onto the Bell state as an example, their idea is to decompose the projector into the sum of its stabilizers as $\hat{P}_{\text{Bell}} = \sum_{i=1}^4 \hat{S}_i \otimes \hat{S}_i / 4$ with $\hat{S}_i \otimes \hat{S}_i \in \mathbb{S} = \{\hat{I} \otimes \hat{I}, \hat{X} \otimes \hat{X}, -\hat{Y} \otimes \hat{Y}, \hat{Z} \otimes \hat{Z}\}$ and implementing Monte-Carlo sampling to estimate each term in $\hat{P}_{\text{Bell}} \rho_{\text{noisy}} \hat{P}_{\text{Bell}}$ as follows. Suppose we want to estimate the expectation value of observable \hat{O} for the projected state after applying a completely positive trace-preserving (CPTP) map \mathcal{V} . The expectation value from measuring \hat{X} on $|+\rangle$ shown in Fig. 1(b) and \hat{O} on the target state after applying the CPTP map is $\langle \hat{X} \otimes \hat{O} \rangle_{ij} = \text{Tr}[\hat{O} \mathcal{V}((\hat{S}_i \otimes \hat{S}_i) \rho_{\text{noisy}} (\hat{S}_i \hat{S}_j \otimes \hat{S}_i \hat{S}_j) + \text{h.c.})] / 2$. Additionally, as part of the same experimental setup, we can simultaneously estimate $\langle \hat{X} \otimes \hat{I} \rangle_{ij}$ by disregarding the measurement of \hat{O} . The desired expectation value, $\text{Tr}[\hat{O} \mathcal{V}(\rho_{\text{Bell}})]$, is obtained by dividing the averages of

these expectation values over the stabilizer group \mathbb{S} as

$$\frac{\frac{1}{16} \sum_{i,j=1}^4 \langle \hat{X} \otimes \hat{O} \rangle_{ij}}{\frac{1}{16} \sum_{i,j=1}^4 \langle \hat{X} \otimes \hat{I} \rangle_{ij}} = \frac{\text{Tr}[\hat{O} \mathcal{V}(\hat{P}_{\text{Bell}} \rho_{\text{noisy}} \hat{P}_{\text{Bell}})]}{\text{Tr}[\hat{P}_{\text{Bell}} \rho_{\text{noisy}} \hat{P}_{\text{Bell}}]}, \quad (1)$$

where $\hat{S}_i \hat{S}_j \otimes \hat{S}_i \hat{S}_j = \hat{S}_k \otimes \hat{S}_k \in \mathbb{S}$ are used. In this way, given the expectation value as the goal, we can treat (virtually) purified states as real purified states in conventional purification.

Our idea is to implement this virtual projection by replacing the non-local controlled operation in Fig. 1(b) with the noisy-entanglement ancilla state and local controlled operations for DQC (Fig. 1(c)). Preparing the Bell state ancilla allows us to implement the same procedure above by replacing the \hat{X} measurement on the $|+\rangle$ in Fig. 1(b) with $\hat{X} \otimes \hat{X}$ measurement on $\rho_{\text{ancilla}} = \rho_{\text{Bell}}$ in Fig. 1(c). Although we find that some kinds of noisy entangled states, including a Werner state or a Bell state with amplitude damping or dephasing noise, reduce the expectation value by a constant factor, as shown in Supplementary Materials (SM) [59]; this yields the desired expectation value since this factor vanishes by the division in Eq. (1). Indeed, this can be seen as a virtual version of conventional recurrence protocols [37, 39, 41, 42, 60] due to its construction; see Fig. 1.

For general settings, suppose we want to implement a quantum computation that outputs $\text{Tr}[\hat{O} \mathcal{U}(\rho_{\text{in}})]$, where \hat{O} is a local operator, \mathcal{U} is a CPTP map including n non-local two-qubit operations acting on some input state ρ_{in} . In DQC, these non-local operations are realized by state and gate teleportation with the consumption of n Bell states, and the desired expectation value is

$\text{Tr}[\hat{O}\mathcal{U}_{\text{dqc}}(\rho_{\text{in}} \otimes \rho_{\text{Bell}}^{\otimes n})]$, where \mathcal{U}_{dqc} is a CPTP operation including n teleportations that consume $\rho_{\text{Bell}}^{\otimes n}$ to realize n non-local two-qubit operations; note that we can prepare only noisy Bell states in typical DQC. As described below, our protocol provides the desired expectation value by virtually purifying n noisy Bell states, $\bigotimes_{\ell=1}^n \rho_{\text{noisy}}^{(\ell)}$ with $\rho_{\text{noisy}}^{(\ell)}$ being the ℓ -th noisy state, using additional n noisy entangled ancilla states. To ensure the generality of our protocol, we use a Werner state with infidelity ϵ as an entangled ancilla state, $\rho_{\text{ancilla}} = \rho_{\text{Werner}} = (1 - 4\epsilon/3)\rho_{\text{Bell}} + \epsilon\hat{I}/3$, because this state can, by suitable twirling operations, be prepared from any two-qubit state without changing its fidelity [60]. The complete protocol is as follows:

1. In preparation for the p -th circuit run, Alice and Bob share $2n$ noisy Bell states and make n Werner states by twirling n noisy Bell states out of $2n$. They uniformly sample the indices $i_\ell, j_\ell = 1, 2, 3, 4$ with $\ell = 1, \dots, n$ for purifying the ℓ -th noisy Bell state and share them by classical communication.
2. They run the quantum circuit \mathcal{U}_{dqc} for input state ρ_{in} , where they use the purification circuit in Fig. 1(c) to generate n (virtually) purified Bell states and consume them for n non-local two-qubit operations.
3. They classically communicate their measurement results and record the results of $(\bigotimes_{\ell=1}^n \hat{X}^{(\ell)} \otimes \hat{X}^{(\ell)}) \otimes \hat{O}$ as a_p and $(\bigotimes_{\ell=1}^n \hat{X}^{(\ell)} \otimes \hat{X}^{(\ell)}) \otimes \hat{I}$ as b_p , where $\hat{X}^{(\ell)} \otimes \hat{X}^{(\ell)}$ denotes the $\hat{X} \otimes \hat{X}$ measurement on the ℓ -th Werner state ancilla.
4. They repeat the procedures above N times and calculate their averages as $a = \sum_p a_p/N$ and $b = \sum_p b_p/N$.
5. Output a/b , which provides the desired expectation value of $\text{Tr}[\hat{O}\mathcal{U}_{\text{dqc}}(\rho_{\text{in}} \otimes \rho_{\text{Bell}}^{\otimes n})]$ as

$$\frac{\text{Tr}[\hat{O}\mathcal{U}_{\text{dqc}}(\rho_{\text{in}} \otimes \bigotimes_{\ell=1}^n (\hat{P}_{\text{Bell}}^{(\ell)} \rho_{\text{noisy}}^{(\ell)} \hat{P}_{\text{Bell}}^{(\ell)}))]}{\text{Tr}[\bigotimes_{\ell=1}^n (\hat{P}_{\text{Bell}}^{(\ell)} \rho_{\text{noisy}}^{(\ell)} \hat{P}_{\text{Bell}}^{(\ell)})]}, \quad (2)$$

where $\hat{P}_{\text{Bell}}^{(\ell)}$ is the projector on the ideal Bell state for the ℓ -th noisy state. Since division by b , which is an estimator of $[\prod_{\ell=1}^n (1 - 4\epsilon^{(\ell)}/3)]\text{Tr}[\bigotimes_{\ell=1}^n (\hat{P}_{\text{Bell}}^{(\ell)} \rho_{\text{noisy}}^{(\ell)})]$, with $\epsilon^{(\ell)}$ being a infidelity of the ℓ -th Werner state ancilla, increases the variance of a/b by $1/b^2$, we need $[\gamma(n)]^2$ more sampling of the noisy circuit run [58, 61], where

$$\gamma(n) = \prod_{\ell=1}^n \gamma^{(\ell)} = \prod_{\ell=1}^n \left(1 - \frac{4}{3}\epsilon^{(\ell)}\right)^{-1} (F_{\text{noisy}}^{(\ell)})^{-1}, \quad (3)$$

is the sampling-cost factor with $F_{\text{noisy}}^{(\ell)} = \text{Tr}[\hat{P}_{\text{Bell}}^{(\ell)} \rho_{\text{noisy}}^{(\ell)} \hat{P}_{\text{Bell}}^{(\ell)}]$ being the fidelity of the ℓ -th noisy state.

Instead of n Werner states, we can repeatedly use just one Werner ancilla state as shown in Fig. 1(d). This reduces the sampling-cost factor by $\gamma(n) = (1 - 4\epsilon/3)^{-1} \prod_{\ell=1}^n (F_{\text{noisy}}^{(\ell)})^{-1}$ with ϵ being the infidelity of a

Werner state ancilla if we can neglect temporal decoherence i.e. for sufficiently short ancilla reuse times, and therefore greater efficiency is possible. Moreover, as we will discuss later, replacing all entanglement states with suitable separable states and additional measurements produces an asymptotically optimal circuit knitting.

Comparison with conventional purification.

The performance of conventional entanglement purification protocols is evaluated using the metric of yield $Y(F_{\text{purified}}, F_{\text{noisy}})$ defined as the ratio between the number of purified and noisy Bell states with fidelity of F_{purified} and F_{noisy} , respectively. Yield can be written as $Y(F_{\text{purified}}, F_{\text{noisy}}) = \prod_{i=1}^{n_{\text{round}}(F_{\text{purified}})} [p_i(F_{i-1})/K_i]$, where $n_{\text{round}}(F_{\text{purified}})$ is the number of purification rounds required to achieve F_{purified} , and K_i is the number of noisy Bell states consumed in the i -th round. Here, $p_i(F_{i-1})$ is the success probability of the i -th purification round using the $(i-1)$ -th noisy Bell state with a fidelity of F_{i-1} , where $F_0 = F_{\text{noisy}}$ [39, 41, 43, 62].

To evaluate the performance of our virtual protocol, we extend the definition of yield to suit virtual purification protocols. As virtual protocols increase sampling overhead by a factor of $[\gamma(n)]^2$ to achieve the same accuracy of non-virtual protocols [58, 61], we define the yield for our protocol as

$$Y_{\text{virtual}} = \prod_{i=1}^{n_{\text{round}}(F_{\text{purified}})} \frac{1}{K_i} \prod_{\ell=1}^n \frac{1}{[\gamma^{(\ell)}]^2}. \quad (4)$$

Note that, since usual virtual protocols are constructed to obtain the expectation value of \hat{O} with the (virtually) purified state ρ_{purified} , the entanglement fidelity [39, 62], defined as $F_{\text{purified}} = \text{Tr}[\hat{P}_{\text{Bell}} \rho_{\text{purified}}] / \text{Tr}[\rho_{\text{purified}}]$, is obtained by setting $\hat{O} = \hat{P}_{\text{Bell}}$. In this way, F_{purified} is calculated by implementing the Bell measurement on the (virtually) purified states in the following numerical simulation for our protocol and PEC: see also the quantum circuit in SM [59]. We numerically calculated their purified fidelity and the corresponding yield using Qulacs [65]. For simplicity, we set $\rho_{\text{noisy}}^{(\ell)} = \rho_{\text{Werner}}$ with an initial fidelity of $F_{\text{noisy}}^{(\ell)} = 1 - \epsilon^{(\ell)} = 0.9$ for all ℓ . We chose the double-selection protocol [41] as a benchmark because it can be seen as the non-virtual equivalent of ours (see Fig. 1). We introduced the following local noise: single-qubit depolarizing noise after each single-qubit gate, $\mathcal{E}_1(\rho) = (1 - 4p_1/3)\rho + (4p_1/3)\sum_{\hat{P}=\hat{I},\hat{X},\hat{Y},\hat{Z}} \hat{P}\rho\hat{P}/4$ with $p_1 = 0.001$, two-qubit depolarizing noise after each two-qubit gate, $\mathcal{E}_2(\rho) = (1 - 16/15p_2)\rho + (16/15p_2)\sum_{\hat{P}_1, \hat{P}_2=\hat{I},\hat{X},\hat{Y},\hat{Z}} (\hat{P}_1 \otimes \hat{P}_2)\rho(\hat{P}_1 \otimes \hat{P}_2)/16$ with $p_2 = 0.01$, and readout error before each \hat{X} measurement, $\mathcal{E}_{\text{mes}}(\rho) = (1 - p_{\text{mes}})\rho + p_{\text{mes}}\hat{Z}\rho\hat{Z}$ with $p_{\text{mes}} = 0.03$.

Figure 2 (a) shows the purified fidelity and the corresponding yield. Note that we use the geometrical-mean fidelity, $F_{\text{purified}}^{1/n}$, as the purified fidelity for our virtual protocol. As shown, our virtual protocol with and with-

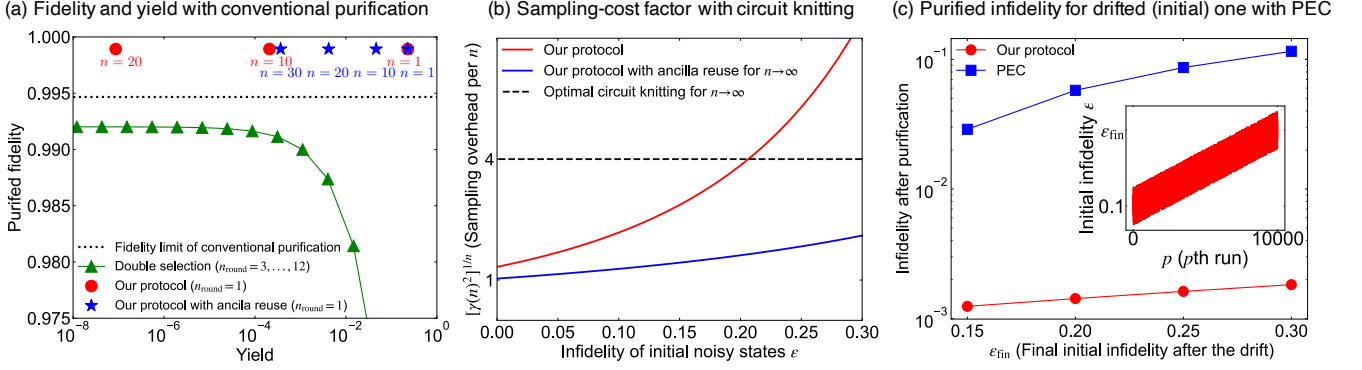


FIG. 2. (a) Purified fidelity with the corresponding yield for our protocol with and without ancilla reuse (the blue stars and red circles, respectively) and conventional double-selection protocol (the green curve with triangles). The black dotted line shows the upper limit of the fidelity achievable by conventional protocols [41, 42]. We consider the geometric-mean fidelity for multiple n . (b) Sampling overhead per purified Bell state, $[\gamma(n)^2]^{1/n}$, with the initial infidelity ϵ of the input noisy states and Werner ancilla states for our protocol. The black dotted horizontal lines represent the lower bounds for circuit knitting for $n = \infty$, $[\gamma(n)^2]^{1/n} = [(2^{n+1} - 1)^2]^{1/n}$ [32, 63, 64]. (c) Infidelity after purification for our protocol and a simple Pauli PEC with the noisy input state $\tilde{\rho}_{\text{noisy}}^{(\ell)} = \frac{1}{N} \sum_p \rho_p^{(\ell)}$, where $\rho_p^{(\ell)}$ is the Werner state for the p -th run with its infidelity drifted as shown in the inset.

out ancilla reuse achieves a fidelity of 99.9%, much higher than the maximum fidelity of the double-selection protocol. Although the yield for our protocol exponentially decreases with increasing n , it is comparable to the yield for the double-selection protocol for a few tens of n . Remarkably, the purified fidelity of our protocol also surpasses the upper fidelity limit of 99.5% for conventional protocols with $p_2 = 0.01$ [41, 42]. This is due to the effect of local two-qubit noise on the virtual state at the expectation value level in our virtual protocol, which is different from that on the real state in conventional purification protocols. The fidelity limit of conventional protocols comes from local two-qubit errors that cannot be detected by one-shot measurements on the ancillae. These errors include ones that do not affect the ancillae but rather the target states, such as $\hat{I} \otimes \hat{P}$ ($\hat{P} = \hat{X}, \hat{Y}, \hat{Z}$). In addition, at least one kind of error cannot be detected intrinsically; see Refs. [41, 42] for details. Therefore, both Alice and Bob experience four errors of 15 kinds of local two-qubit errors that cannot be detected, leading to an infidelity limit of $4p_2/15 \times 2$ [41, 42]. Meanwhile, in our virtual protocol, the two-qubit errors simply reduce the amplitude of the expectation value, and the leading-order term of $\mathcal{O}(p_2)$ vanishes due to the division in Eq. (2), resulting in purified Bell states with leading-order infidelity term of $\frac{8}{15}p_2\epsilon$. A detailed analysis of this and other noises is left to SM [59].

Comparison with circuit knitting.— Circuit knitting simulates entanglement with only separable-state preparation and LOCC, but requires more sampling to achieve the same accuracy. To simulate n Bell states using circuit knitting, we first decompose $\rho_{\text{Bell}}^{\otimes n} = \sum_i c_i \mathcal{U}_{\text{LOCC},i}(\rho_{\text{sep},i}) = \gamma(n) \sum_i p_i \mathcal{U}_{\text{LOCC},i}(\rho_{\text{sep},i})$, where c_i is a coefficient, $\mathcal{U}_{\text{LOCC},i}$ is a CPTP map confined to LOCC, $\rho_{\text{sep},i}$ is a separable state, $\gamma(n) = \sum_i |c_i|$,

and $p_i = \text{sgn}(c_i)|c_i|/\gamma(n)$ is a probability distribution. We can thus simulate $\rho_{\text{Bell}}^{\otimes n}$ by summing up the results of the outcome obtained by Monte-Carlo sampling with the probability distribution $\{p_i\}$ and multiplied by $\gamma(n)\text{sgn}(c_i)$.

Figure 2 (b) compares the sampling overhead per Bell state, $[\gamma(n)^2]^{1/n}$, for our protocol with that for the optimal one for circuit knitting, $\gamma(n) = 2^{n+1} - 1$ [32, 63, 64]. The numerical setup, including local noise, is the same as that with conventional purification. Our protocol shows a much lower sampling overhead than optimal circuit knitting for reasonable initial infidelity. For example, a 10% infidelity of initial Werner states, which may be achievable with current technologies [19, 20, 22, 24–30], yields $[\gamma(n)^2]^{1/n}$ that is around half of that for optimal circuit knitting, leading to a reduction in total sampling overhead of around $(1/2)^n$ for simulating n purified Bell states. This reduction offered by our protocol comes from its use of noisy entanglement as a resource. Our protocol thus can be seen as an extended variant of circuit knitting that utilizes entanglement.

Finally, we note that we can produce an asymptotically optimal circuit-knitting protocol from our protocol with ancilla reuse, by implementing $\hat{X} \otimes \hat{X}$ and $\hat{Y} \otimes \hat{Y}$ measurements on $|+\rangle \otimes |+\rangle$ ancilla instead of $\hat{X} \otimes \hat{X}$ on a noisy entanglement ancilla as well as considering initial states as separable states such as $|0\rangle \otimes |0\rangle$: see Fig. 1. As shown in SM [59], the additional measurement of $\hat{Y} \otimes \hat{Y}$ doubles $\gamma(n)$, and the fidelity of $|0\rangle \otimes |0\rangle$ to ρ_{Bell} is $F_{\text{noisy}}^{(\ell)} = 1/2$, leading to $\gamma(n) = 2^{n+1}$.

Using this approach, we can construct an asymptotically optimal circuit-knitting protocol that inherits the noise-resilient properties of our original protocol.

Robustness to the drift in initial-state infidelity.— Our protocol is robust against the drift of initial

infidelity because it effectively projects the state onto the symmetric subspace for the stabilizers, \mathcal{S} . Denote the ℓ -th initial noisy state in the p -th experimental run as $\rho_p^{(\ell)}$ and the total number of experimental runs as N . The expectation value in the presence of drifted noise is given by

$$\frac{\text{Tr}[\hat{\mathcal{O}}_{\text{dqc}}(\rho_{\text{in}} \otimes (\bigotimes_{\ell=1}^n \hat{P}_{\text{Bell}}^{(\ell)} \bar{\rho}_{\text{noisy}}^{(\ell)} \hat{P}_{\text{Bell}}^{(\ell)})]}{\text{Tr}[\bigotimes_{\ell=1}^n \hat{P}_{\text{Bell}}^{(\ell)} \bar{\rho}_{\text{noisy}}^{(\ell)} \hat{P}_{\text{Bell}}^{(\ell)}]}}, \quad (5)$$

where $\bar{\rho}_{\text{noisy}}^{(\ell)} = \frac{1}{N} \sum_p \rho_p^{(\ell)}$. This implies that our virtual protocol works for the averaged state $\bar{\rho}_{\text{noisy}}^{(\ell)}$. Using this averaged state, we conducted a numerical experiment for our protocol and a simple Pauli PEC, which requires error information; see details of this PEC in SM [59]. The numerical demonstration considers the initial infidelity drift from 0.1 to ϵ_{fin} as $\epsilon_p = 0.1 + (\epsilon_{\text{fin}} - 0.1)p/N$ with uniform random fluctuation between $[-0.05, 0.05]$, while the estimated ϵ for PEC is assumed to be 0.1; see the inset of Fig. 2(c). We use the same noise for comparison with conventional purification. With these parameters, we construct the initial average noisy state $\bar{\rho}_{\text{noisy}}^{(\ell)}$ with $N = 10^4$ and calculate the purified infidelity for our protocol and PEC, as shown in Fig. 2(c). As shown, our protocol shows much better robustness to the drift in initial infidelity than PEC.

Conclusion and outlook.— We have proposed a virtual entanglement purification protocol for DQC that purifies noisy Bell states at the expectation value level. We have demonstrated its advantages over conventional entanglement purification, circuit knitting, and PEC for noisy Bell states: surpasses the fidelity limit in the pres-

ence of noise in LOCC, requires fewer sampling shots, and exhibits robustness against initial infidelity fluctuations in shared entanglement. As a byproduct, we have also proposed an asymptotically optimal circuit-knitting protocol that may inherit the noise-resilient properties of our original protocol. Our protocol bridges the gap between entanglement purification and circuit knitting, and so provides a flexible approach to DQC. We may combine virtual purification flexibly with conventional entanglement purification and other error mitigation techniques.

Future work includes the extension of our virtual protocol for multiple entangled states such as the GHZ and linear cluster states. Moreover, the technique of replacing non-local controlled operations with noisy entanglement preparation and local controlled operations for DQC can be applied to the generalized Hadamard test as shown in SM [59]. Since the Hadamard test is a building block for many error mitigation protocols or quantum computation algorithms [66] including the single-ancilla linear combination of unitaries [67], this replacement may be useful when applying such protocols or algorithms for DQC.

ACKNOWLEDGMENTS

Acknowledgments.— This work was supported by JST [Moonshot R&D] Grant Nos. JPMJMS2061 and JPMJMS226C; JST, PRESTO, Grant No. JPMJPR2114, Japan; MEXT Q-LEAP, Grant Nos. JPMXS0120319794 and JPMXS0118068682; JST CREST Grant No. JPMJCR23I4; JSPS KAKENHI, Grant No. 23H04390. This work was supported by JST Moonshot (Grant Number JPMJMS226C). Y. M. is supported by JSPS KAKENHI (Grant Number 23H04390) and PREST, JST. This work was also supported by CREST (JPMJCR23I5), JST.

* kaoru.yamamoto@ntt.com

† suguru.endou@ntt.com

- [1] C. Cabrillo, J. I. Cirac, P. García-Fernández, and P. Zoller, “Creation of entangled states of distant atoms by interference,” *Phys. Rev. A* **59**, 1025–1033 (1999).
- [2] S. Bose, P. L. Knight, M. B. Plenio, and V. Vedral, “Proposal for teleportation of an atomic state via cavity decay,” *Phys. Rev. Lett.* **83**, 5158–5161 (1999).
- [3] S C Benjamin, J Eisert, and T M Stace, “Optical generation of matter qubit graph states,” *New J. Phys.* **7**, 194 (2005).
- [4] C. W. Chou, H. de Riedmatten, D. Felinto, S. V. Polyakov, S. J. van Enk, and H. J. Kimble, “Measurement-induced entanglement for excitation stored in remote atomic ensembles,” *Nature (London)* **438**, 828–832 (2005).
- [5] Yuan Liang Lim, Almut Beige, and Leong Chuan Kwek, “Repeat-until-success linear optics distributed quantum computing,” *Phys. Rev. Lett.* **95**, 030505 (2005).
- [6] Sean D. Barrett and Pieter Kok, “Efficient high-fidelity quantum computation using matter qubits and linear optics,” *Phys. Rev. A* **71**, 060310 (2005).
- [7] Simon C Benjamin, Daniel E Browne, Joe Fitzsimons, and John J L Morton, “Brokered graph-state quantum computation,” *New J. Phys.* **8**, 141 (2006).
- [8] D. L. Moehring, P. Maunz, S. Olmschenk, K. C. Younge, D. N. Matsukevich, L. M. Duan, and C. Monroe, “Entanglement of single-atom quantum bits at a distance,” *Nature (London)* **449**, 68–71 (2007).
- [9] S.C. Benjamin, B.W. Lovett, and J.M. Smith, “Prospects for measurement-based quantum computing with solid state spins,” *Laser & Photonics Reviews* **3**, 556–574 (2009).
- [10] Yu-Bo Sheng, Fu-Guo Deng, and Gui Lu Long, “Complete hyperentangled-bell-state analysis for quantum communication,” *Phys. Rev. A* **82**, 032318 (2010).
- [11] Naomi H. Nickerson, Joseph F. Fitzsimons, and Simon C. Benjamin, “Freely scalable quantum technologies using cells of 5-to-50 qubits with very lossy and noisy photonic links,” *Phys. Rev. X* **4**, 041041 (2014).
- [12] Ramil Nigmatullin, Christopher J Ballance, Niel de Beaudrap, and Simon C Benjamin, “Minimally com-

- plex ion traps as modules for quantum communication and computing,” *New J. Phys.* **18**, 103028 (2016).
- [13] Xiao-Min Hu, Cen-Xiao Huang, Yu-Bo Sheng, Lan Zhou, Bi-Heng Liu, Yu Guo, Chao Zhang, Wen-Bo Xing, Yun-Feng Huang, Chuan-Feng Li, and Guang-Can Guo, “Long-distance entanglement purification for quantum communication,” *Phys. Rev. Lett.* **126**, 010503 (2021).
- [14] Sergey Bravyi, Oliver Dial, Jay M. Gambetta, Dario Gil, and Zaira Nazario, “The future of quantum computing with superconducting qubits,” *J. Appl. Phys.* **132**, 160902 (2022).
- [15] James Ang, Gabriella Carini, Yanzhu Chen, Isaac Chuang, Michael Austin DeMarco, Sophia E Economou, Alec Eickbusch, Andrei Faraon, Kai-Mei Fu, Steven M Girvin, et al., “Architectures for multinode superconducting quantum computers,” arXiv:2212.06167 (2022).
- [16] Hamza Jnane, Brennan Undseth, Zhenyu Cai, Simon C. Benjamin, and Bálint Koczor, “Multicore quantum computing,” *Phys. Rev. Appl.* **18**, 044064 (2022).
- [17] Marcello Caleffi, Michele Amoretti, Davide Ferrari, Jessica Illiano, Antonio Manzalini, and Angela Sara Cacciapuoti, “Distributed quantum computing: A survey,” *Computer Networks* **254**, 110672 (2024).
- [18] P. Kurpiers, P. Magnard, T. Walter, B. Royer, M. Pechal, J. Heinsoo, Y. Salathé, A. Akin, S. Storz, J. C. Besse, S. Gasparinetti, A. Blais, and A. Wallraff, “Deterministic quantum state transfer and remote entanglement using microwave photons,” *Nature* **558**, 264–267 (2018).
- [19] Kevin S. Chou, Jacob Z. Blumoff, Christopher S. Wang, Philip C. Reinhold, Christopher J. Axline, Yvonne Y. Gao, L. Frunzio, M. H. Devoret, Liang Jiang, and R. J. Schoelkopf, “Deterministic teleportation of a quantum gate between two logical qubits,” *Nature (London)* **561**, 368–373 (2018).
- [20] P. Campagne-Ibarcq, E. Zolys-Geller, A. Narla, S. Shankar, P. Reinhold, L. Burkhardt, C. Axline, W. Pfaff, L. Frunzio, R. J. Schoelkopf, and M. H. Devoret, “Deterministic remote entanglement of superconducting circuits through microwave two-photon transitions,” *Phys. Rev. Lett.* **120**, 200501 (2018).
- [21] Y. P. Zhong, H. S. Chang, K. J. Satzinger, M. H. Chou, A. Bienfait, C. R. Conner, É. Dumur, J. Grebel, G. A. Peairs, R. G. Povey, D. I. Schuster, and A. N. Cleland, “Violating bell’s inequality with remotely connected superconducting qubits,” *Nat. Phys.* **15**, 741–744 (2019).
- [22] B. Kannan, D. L. Campbell, F. Vasconcelos, R. Winik, D. K. Kim, M. Kjaergaard, P. Krantz, A. Melville, B. M. Niedzielski, J. L. Yoder, T. P. Orlando, S. Gustavsson, and W. D. Oliver, “Generating spatially entangled itinerant photons with waveguide quantum electrodynamics,” *Science Advances* **6**, eabb8780 (2020).
- [23] Youpeng Zhong, Hung-Shen Chang, Audrey Bienfait, Étienne Dumur, Ming-Han Chou, Christopher R. Conner, Joel Grebel, Rhys G. Povey, Haoxiong Yan, David I. Schuster, and Andrew N. Cleland, “Deterministic multi-qubit entanglement in a quantum network,” *Nature (London)* **590**, 571–575 (2021).
- [24] Severin Daiss, Stefan Langenfeld, Stephan Welte, Emanuele Distanto, Philip Thomas, Lukas Hartung, Olivier Morin, and Gerhard Rempe, “A quantum-logic gate between distant quantum-network modules,” *Science* **371**, 614–617 (2021).
- [25] Tim van Leent, Matthias Bock, Florian Fertig, Robert Garthoff, Sebastian Eppelt, Yiru Zhou, Pooja Malik, Matthias Seubert, Tobias Bauer, Wenjamin Rosenfeld, Wei Zhang, Christoph Becher, and Harald Weinfurter, “Entangling single atoms over 33 km telecom fibre,” *Nature (London)* **607**, 69–73 (2022).
- [26] Xi-Yu Luo, Yong Yu, Jian-Long Liu, Ming-Yang Zheng, Chao-Yang Wang, Bin Wang, Jun Li, Xiao Jiang, Xiuping Xie, Qiang Zhang, Xiao-Hui Bao, and Jian-Wei Pan, “Postselected entanglement between two atomic ensembles separated by 12.5 km,” *Phys. Rev. Lett.* **129**, 050503 (2022).
- [27] N. Leung, Y. Lu, S. Chakram, R. K. Naik, N. Earnest, R. Ma, K. Jacobs, A. N. Cleland, and D. I. Schuster, “Deterministic bidirectional communication and remote entanglement generation between superconducting qubits,” *npj Quantum Information* **5**, 18 (2019).
- [28] Haoxiong Yan, Youpeng Zhong, Hung-Shen Chang, Audrey Bienfait, Ming-Han Chou, Christopher R. Conner, Étienne Dumur, Joel Grebel, Rhys G. Povey, and Andrew N. Cleland, “Entanglement purification and protection in a superconducting quantum network,” *Phys. Rev. Lett.* **128**, 080504 (2022).
- [29] Ming Lai Chan, Alexey Tiranov, Martin Hayhurst Appel, Ying Wang, Leonardo Midolo, Sven Scholz, Andreas D. Wieck, Arne Ludwig, Anders Søndberg Sørensen, and Peter Lodahl, “On-chip spin-photon entanglement based on photon-scattering of a quantum dot,” *npj Quantum Information* **9**, 49 (2023).
- [30] Jiawei Qiu, Yang Liu, Jingjing Niu, Ling Hu, Yukai Wu, Libo Zhang, Wenhui Huang, Yuanzhen Chen, Jian Li, Song Liu, et al., “Deterministic quantum teleportation between distant superconducting chips,” arXiv:2302.08756 (2023).
- [31] Joel Grebel, Haoxiong Yan, Ming-Han Chou, Gustav Andersson, Christopher R. Conner, Yash J. Joshi, Jacob M. Miller, Rhys G. Povey, Hong Qiao, Xuntao Wu, and Andrew N. Cleland, “Bidirectional multiphoton communication between remote superconducting nodes,” *Phys. Rev. Lett.* **132**, 047001 (2024).
- [32] Christophe Piveteau and David Sutter, “Circuit knitting with classical communication,” *IEEE Transactions on Information Theory*, 1–1 (2023).
- [33] Elisa Bäumer, Vinay Tripathi, Derek S Wang, Patrick Rall, Edward H Chen, Swarnadeep Majumder, Alireza Seif, and Zlatko K Minev, “Efficient long-range entanglement using dynamic circuits,” arXiv:2308.13065 (2023).
- [34] Almudena Carrera Vazquez, Caroline Tornow, Diego Ristè, Stefan Woerner, Maika Takita, and Daniel J. Egger, “Combining quantum processors with real-time classical communication,” *Nature(London)* (2024), 10.1038/s41586-024-08178-2.
- [35] Tian-Ren Jin, Kai Xu, and Heng Fan, “Distributed quantum computation via entanglement forging and teleportation,” arXiv:2409.02509 (2024).
- [36] Giuseppe Bisicchia, Giuseppe Clemente, Jose Garcia-Alonso, Juan Manuel Murillo Rodríguez, Massimo D’Elia, and Antonio Brogi, “Distributing quantum computations, shot-wise,” arXiv:2411.16530 (2024).
- [37] Charles H. Bennett, Gilles Brassard, Sandu Popescu, Benjamin Schumacher, John A. Smolin, and William K. Wootters, “Purification of noisy entanglement and faithful teleportation via noisy channels,” *Phys. Rev. Lett.* **76**, 722–725 (1996).
- [38] David Deutsch, Artur Ekert, Richard Jozsa, Chiara Mac-

- chiavello, Sandu Popescu, and Anna Sanpera, “Quantum privacy amplification and the security of quantum cryptography over noisy channels,” *Phys. Rev. Lett.* **77**, 2818–2821 (1996).
- [39] W Dür and H J Briegel, “Entanglement purification and quantum error correction,” *Rep. Prog. Phys.* **70**, 1381 (2007).
- [40] Yu-Bo Sheng and Fu-Guo Deng, “Deterministic entanglement purification and complete nonlocal bell-state analysis with hyperentanglement,” *Phys. Rev. A* **81**, 032307 (2010).
- [41] Keisuke Fujii and Katsuji Yamamoto, “Entanglement purification with double selection,” *Phys. Rev. A* **80**, 042308 (2009).
- [42] Stefan Krastanov, Victor V. Albert, and Liang Jiang, “Optimized Entanglement Purification,” *Quantum* **3**, 123 (2019).
- [43] F. Riera-Sàbat, P. Sekatski, A. Pirker, and W. Dür, “Entanglement-assisted entanglement purification,” *Phys. Rev. Lett.* **127**, 040502 (2021).
- [44] Stefan Krastanov, Alexander Sanchez de la Cerda, and Prineha Narang, “Heterogeneous multipartite entanglement purification for size-constrained quantum devices,” *Phys. Rev. Res.* **3**, 033164 (2021).
- [45] Kenneth Goodenough, Sebastian De Bone, Vaishnavi Addala, Stefan Krastanov, Sarah Jansen, Dion Gijswijt, and David Elkouss, “Near-term n to k distillation protocols using graph codes,” *IEEE Journal on Selected Areas in Communications*, 1–1 (2024).
- [46] Charles H. Bennett, Gilles Brassard, Claude Crépeau, Richard Jozsa, Asher Peres, and William K. Wootters, “Teleporting an unknown quantum state via dual classical and einstein-podolsky-rosen channels,” *Phys. Rev. Lett.* **70**, 1895–1899 (1993).
- [47] J. Eisert, K. Jacobs, P. Papadopoulos, and M. B. Plenio, “Optimal local implementation of nonlocal quantum gates,” *Phys. Rev. A* **62**, 052317 (2000).
- [48] S. Pirandola, J. Eisert, C. Weedbrook, A. Furusawa, and S. L. Braunstein, “Advances in quantum teleportation,” *Nat. Photonics* **9**, 641–652 (2015).
- [49] Xiao-Min Hu, Yu Guo, Bi-Heng Liu, Chuan-Feng Li, and Guang-Can Guo, “Progress in quantum teleportation,” *Nat. Rev. Phys.* **5**, 339–353 (2023).
- [50] Jun-Yi Wu, Kosuke Matsui, Tim Forrer, Akihito Soeda, Pablo Andrés-Martínez, Daniel Mills, Luciana Henaut, and Mio Muraō, “Entanglement-efficient bipartite-distributed quantum computing,” *Quantum* **7**, 1196 (2023).
- [51] Youngseok Kim, Andrew Eddins, Sajant Anand, Ken Xuan Wei, Ewout van den Berg, Sami Rosenblatt, Hasan Nayfeh, Yantao Wu, Michael Zaletel, Kristan Temme, and Abhinav Kandala, “Evidence for the utility of quantum computing before fault tolerance,” *Nature* **618**, 500–505 (2023).
- [52] Suguru Endo, Zhenyu Cai, Simon C. Benjamin, and Xiao Yuan, “Hybrid quantum-classical algorithms and quantum error mitigation,” *J. Phys. Soc. Jpn.* **90**, 032001 (2021).
- [53] Zhenyu Cai, Ryan Babbush, Simon C. Benjamin, Suguru Endo, William J. Huggins, Ying Li, Jarrod R. McClean, and Thomas E. O’Brien, “Quantum error mitigation,” *Rev. Mod. Phys.* **95**, 045005 (2023).
- [54] Xiao Yuan, Bartosz Regula, Ryuji Takagi, and Mile Gu, “Virtual quantum resource distillation,” *Phys. Rev. Lett.* **132**, 050203 (2024).
- [55] Ting Zhang, Yukun Zhang, Lu Liu, Xiao-Xu Fang, Qian-Xi Zhang, Xiao Yuan, and He Lu, “Experimental virtual distillation of entanglement and coherence,” *arXiv* (2023), 2311.09874 [quant-ph].
- [56] Ryuji Takagi, Xiao Yuan, Bartosz Regula, and Mile Gu, “Virtual quantum resource distillation: General framework and applications,” *Phys. Rev. A* **109**, 022403 (2024).
- [57] Michael A Nielsen and Isaac Chuang, “Quantum computation and quantum information,” (2002).
- [58] Kento Tsubouchi, Yasunari Suzuki, Yuuki Tokunaga, Nobuyuki Yoshioka, and Suguru Endo, “Virtual quantum error detection,” *Phys. Rev. A* **108**, 042426 (2023).
- [59] See Supplementary Materials for more details, which includes Refs. [68–73].
- [60] Charles H. Bennett, David P. DiVincenzo, John A. Smolin, and William K. Wootters, “Mixed-state entanglement and quantum error correction,” *Phys. Rev. A* **54**, 3824–3851 (1996).
- [61] Suguru Endo, Yasunari Suzuki, Kento Tsubouchi, Rui Asaoka, Kaoru Yamamoto, Yuichiro Matsuzaki, and Yuuki Tokunaga, “Quantum error mitigation for rotational symmetric bosonic codes with symmetry expansion,” *arXiv*:2211.06164 (2022).
- [62] F. Riera-Sàbat, P. Sekatski, A. Pirker, and W. Dür, “Entanglement purification by counting and locating errors with entangling measurements,” *Phys. Rev. A* **104**, 012419 (2021).
- [63] Lukas Brenner, Christophe Piveteau, and David Sutter, “Optimal wire cutting with classical communication,” *arXiv*:2302.03366 (2023).
- [64] Hiroyuki Harada, Kaito Wada, and Naoki Yamamoto, “Doubly optimal parallel wire cutting without ancilla qubits,” *PRX Quantum* **5**, 040308 (2024).
- [65] Yasunari Suzuki, Yoshiaki Kawase, Yuya Masumura, Yuria Hiraga, Masahiro Nakadai, Jiabao Chen, Ken M. Nakanishi, Kosuke Mitarai, Ryosuke Imai, Shiro Tamiya, Takahiro Yamamoto, Tennin Yan, Toru Kawakubo, Yuya O. Nakagawa, Yohei Ibe, Youyuan Zhang, Hirotsugu Yamashita, Hikaru Yoshimura, Akihiro Hayashi, and Keisuke Fujii, “Qulacs: a fast and versatile quantum circuit simulator for research purpose,” *Quantum* **5**, 559 (2021).
- [66] Lin Lin and Yu Tong, “Heisenberg-limited ground-state energy estimation for early fault-tolerant quantum computers,” *PRX Quantum* **3**, 010318 (2022).
- [67] Shantanav Chakraborty, “Implementing any linear combination of unitaries on intermediate-term quantum computers,” *arXiv*:2302.13555 (2023).
- [68] Jinzhao Sun, Suguru Endo, Huiping Lin, Patrick Hayden, Vlatko Vedral, and Xiao Yuan, “Perturbative quantum simulation,” *Phys. Rev. Lett.* **129**, 120505 (2022).
- [69] Zhenyu Cai, “Quantum Error Mitigation using Symmetry Expansion,” *Quantum* **5**, 548 (2021).
- [70] Kristan Temme, Sergey Bravyi, and Jay M. Gambetta, “Error mitigation for short-depth quantum circuits,” *Phys. Rev. Lett.* **119**, 180509 (2017).
- [71] Suguru Endo, Simon C. Benjamin, and Ying Li, “Practical quantum error mitigation for near-future applications,” *Phys. Rev. X* **8**, 031027 (2018).
- [72] Christophe Piveteau, David Sutter, Sergey Bravyi, Jay M. Gambetta, and Kristan Temme, “Error mitigation for universal gates on encoded qubits,” *Phys. Rev.*

- Lett. **127**, 200505 (2021).
- [73] Yasunari Suzuki, Suguru Endo, Keisuke Fujii, and Yuuki Tokunaga, “Quantum error mitigation as a universal error reduction technique: Applications from the nisq to the fault-tolerant quantum computing eras,” PRX Quantum **3**, 010345 (2022).
- [74] Zhenyu Cai, “Multi-exponential error extrapolation and combining error mitigation techniques for nisq applications,” npj Quantum Information **7**, 80 (2021).

Supplementary Materials for: Virtual entanglement purification via noisy entanglement

CONTENTS

S1. Generalized Hadamard test with noisy entanglement ancilla and local controlled operation	9
A. Bell-diagonal state for the Bell state and a Werner state ancilla	10
B. A Bell state with a local amplitude damping noise	11
C. A Bell state with local dephasing (T_2) noise	11
S2. Using separable ancilla state instead of noisy-entanglement ancilla state	11
S3. Effect of noise in the purification circuit	12
A. Details of numerical calculation	12
B. Analytical validation of the $\frac{8}{15}p_2\epsilon +$ (higher-order terms) infidelity	13
S4. Estimation of fidelity and γ for reusing the Werner state ancilla given $n = 1$ data	16
A. Noiseless purification operations	17
B. Noisy LOCC	18
S5. Probabilistic error cancellation (PEC) for Bell-state preparation using only LOCC	19
A. PEC for Bell-diagonal state	20
B. PEC for a Werner state	21

S1. GENERALIZED HADAMARD TEST WITH NOISY ENTANGLEMENT ANCILLA AND LOCAL CONTROLLED OPERATION

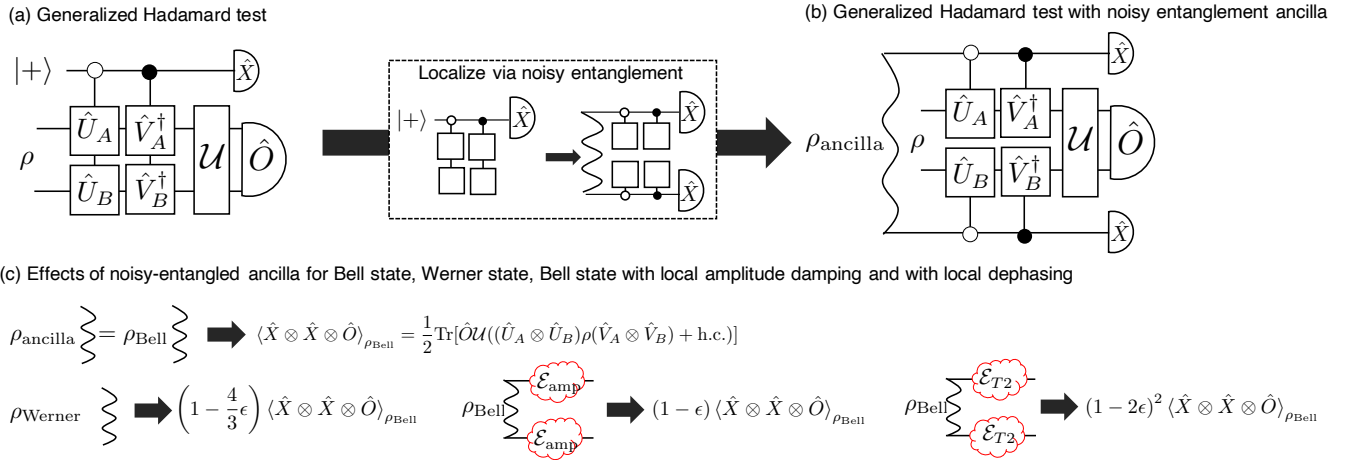


FIG. S1. (a) Generalized Hadamard test, which includes non-local controlled operations. (b) Generalized Hadamard test for DQC by replacing non-local controlled operations with (noisy) entangled ancilla and local controlled operations (c) Effects on the expectation value, $\hat{X} \otimes \hat{X} \otimes \hat{O}$ in (b), with a Bell state ancilla, a Werner state ancilla, a Bell state ancilla with local amplitude damping noise, and a Bell state ancilla with local T_2 noise.

Here, we introduce a generalized Hadamard test for separated subsystems A and B because the generalized Hadamard test is a building block for many quantum algorithms using virtual operations [52, 58, 61, 68], including ours in the main text. Figure S1(a) shows the quantum circuit of a generalized Hadamard test, which requires non-local interaction between subsystems and the ancilla qubit, where ρ is some input state, $\hat{U}_A, \hat{U}_B, \hat{V}_A, \hat{V}_B$ are

some operators, \mathcal{U} is a CPTP map, and \hat{O} is some measurement operator. This circuit simultaneously provides their expectation values as

$$\langle \hat{X} \otimes \hat{O} \rangle = \frac{1}{2} \text{Tr}[\hat{O}\mathcal{U}((\hat{U}_A \otimes \hat{U}_B)\rho(\hat{V}_A \otimes \hat{V}_B) + \text{h.c.})], \quad (\text{S1})$$

$$\langle \hat{X} \otimes \hat{I} \rangle = \frac{1}{2} \text{Tr}[(\hat{U}_A \otimes \hat{U}_B)\rho(\hat{V}_A \otimes \hat{V}_B) + \text{h.c.}]. \quad (\text{S2})$$

By combining this with $\hat{Y} \otimes \hat{O}$ and $\hat{Y} \otimes \hat{I}$ measurement as well as post-processing the measurement data, we can implement various virtual operations at the expectation value level that cannot be attained by physical CPTP maps [52].

We consider the generalized Hadamard test for DQC by replacing the non-local controlled operations in Fig. S1(a) with a (noisy) entanglement ancilla, ρ_{ancilla} , and local controlled operations (Fig. 1(b)). Below, we show that a Bell ancilla state provides the same expectation value as Eq. (S1) and some kinds of noisy Bell states, such as a Werner state or a Bell state with local amplitude damping and dephasing (T_2 noise), simply reduce the expectation value by a constant factor. In many virtual protocols including our protocol, this reduction does not affect the expectation value due to the division in the post-processing for normalizing the unphysical density matrix, as we see in Eq. (2) in the main text.

A. Bell-diagonal state for the Bell state and a Werner state ancilla

Here we consider the Bell-diagonal state, defined as

$$\rho_{\text{diag}} = (1 - \epsilon) |\Psi_{\text{Bell}}\rangle \langle \Psi_{\text{Bell}}| + \epsilon_x |\Psi_x\rangle \langle \Psi_x| + \epsilon_y |\Psi_y\rangle \langle \Psi_y| + \epsilon_z |\Psi_z\rangle \langle \Psi_z| \quad (\text{S3})$$

$$\begin{aligned} &= \frac{1}{2} [(1 - \epsilon + \epsilon_z)(|00\rangle \langle 00| + |11\rangle \langle 11|) + (1 - \epsilon - \epsilon_z)(|00\rangle \langle 11| + |11\rangle \langle 00|) \\ &+ (\epsilon_x + \epsilon_y)(|10\rangle \langle 10| + |01\rangle \langle 01|) + (\epsilon_x - \epsilon_y)(|10\rangle \langle 01| + |01\rangle \langle 10|)], \end{aligned} \quad (\text{S4})$$

where $\epsilon = \epsilon_x + \epsilon_y + \epsilon_z$ and

$$|\Psi_{\text{Bell}}\rangle = \frac{|00\rangle + |11\rangle}{\sqrt{2}}, \quad |\Psi_x\rangle = \frac{|10\rangle + |01\rangle}{\sqrt{2}}, \quad |\Psi_y\rangle = \frac{|10\rangle - |01\rangle}{\sqrt{2}}, \quad |\Psi_z\rangle = \frac{|00\rangle - |11\rangle}{\sqrt{2}}. \quad (\text{S5})$$

Note that $\rho_{\text{diag}} = \rho_{\text{Bell}}$ for $\epsilon = 0$ and $\rho_{\text{diag}} = \rho_{\text{Werner}}$ for $\epsilon_x = \epsilon_y = \epsilon_z = 1/3$. The expectation value of the measurement $\hat{X} \otimes \hat{X} \otimes \hat{O}$ on this state, $\rho_{\text{ancilla}} = \rho_{\text{diag}}$ in Fig. S1(b), is

$$\begin{aligned} \langle \hat{X} \otimes \hat{X} \otimes \hat{O} \rangle &= \frac{1}{2} \text{Tr}[(\hat{X} \otimes \hat{X} \otimes \hat{O})(1 - \epsilon - \epsilon_z)(|00\rangle \langle 11| \otimes \mathcal{U}((\hat{U}_A \otimes \hat{U}_B)\rho(\hat{V}_A \otimes \hat{V}_B)) + \text{h.c.}) \\ &+ (\epsilon_x - \epsilon_y)(|10\rangle \langle 01| \otimes \mathcal{U}((\hat{V}_A^\dagger \otimes \hat{U}_B)\rho(\hat{U}_A^\dagger \otimes \hat{V}_B)) + \text{h.c.}) \\ &+ (\text{other terms unrelated to the } \hat{X} \otimes \hat{X} \text{ measurement})] \end{aligned} \quad (\text{S6})$$

$$= \frac{1}{2} \text{Tr} \left\{ (1 - \epsilon - \epsilon_z)[\hat{O}\mathcal{U}((\hat{U}_A \otimes \hat{U}_B)\rho(\hat{V}_A \otimes \hat{V}_B) + \text{h.c.}) + (\epsilon_x - \epsilon_y)[\hat{O}\mathcal{U}((\hat{V}_A^\dagger \otimes \hat{U}_B)\rho(\hat{U}_A^\dagger \otimes \hat{V}_B) + \text{h.c.})] \right\} \quad (\text{S7})$$

$$= \frac{1}{2} (1 - \epsilon - \epsilon_z) \text{Tr}[\hat{O}\mathcal{U}((\hat{U}_A \otimes \hat{U}_B)\rho(\hat{V}_A \otimes \hat{V}_B) + \text{h.c.})] + \frac{1}{2} (\epsilon_x - \epsilon_y) (\text{bias terms}). \quad (\text{S8})$$

We can immediately see that the Bell state ancilla provides the same expectation value as in Eq. (S1) by setting $\epsilon = \epsilon_x = \epsilon_y = \epsilon_z = 0$,

$$\frac{1}{2} \text{Tr}[\hat{O}\mathcal{U}((\hat{U}_A \otimes \hat{U}_B)\rho(\hat{V}_A \otimes \hat{V}_B) + \text{h.c.})] \equiv \langle \hat{X} \otimes \hat{X} \otimes \hat{O} \rangle_{\rho_{\text{Bell}}}. \quad (\text{S9})$$

By setting $\epsilon_x = \epsilon_y = \epsilon_z = \epsilon/3$, we see that the Werner state ancilla, $\rho_{\text{ancilla}} = \rho_{\text{Werner}}$ provides the expectation value as

$$\langle \hat{X} \otimes \hat{X} \otimes \hat{O} \rangle = \left(1 - \frac{4}{3}\epsilon\right) \langle \hat{X} \otimes \hat{X} \otimes \hat{O} \rangle_{\rho_{\text{Bell}}}. \quad (\text{S10})$$

For the general Bell diagonal state, the bias term in Eq. (S8) vanishes when $\epsilon_x = \epsilon_y$, and we obtain the desired expectation value whose amplitude is reduced by a factor of $(1 - \epsilon - \epsilon_z) \langle \hat{X} \otimes \hat{X} \otimes \hat{O} \rangle_{\rho_{\text{Bell}}}$.

B. A Bell state with a local amplitude damping noise

Here we consider the case where the ideal Bell state ancilla ρ_{Bell} suffers from local amplitude damping noise shown in Fig. S1(b), described as $\mathcal{E}_{\text{amp}}(\rho) = K_0\rho K_0^\dagger + K_1\rho K_1^\dagger$, where

$$K_0 = \begin{pmatrix} 1 & 0 \\ 0 & \sqrt{1-\epsilon} \end{pmatrix}, \quad K_1 = \begin{pmatrix} 0 & \sqrt{\epsilon} \\ 0 & 0 \end{pmatrix}, \quad (\text{S11})$$

are Kraus maps. Since the state is described as

$$(\mathcal{E}_{\text{amp}} \otimes \mathcal{E}_{\text{amp}})(\rho_{\text{Bell}}) = \left(\frac{|00\rangle + (1-\epsilon)|11\rangle}{\sqrt{2}} \right) \left(\frac{\langle 00| + (1-\epsilon)\langle 11|}{\sqrt{2}} \right) + \epsilon(1-\epsilon) \left(\frac{|10\rangle \langle 10|}{\sqrt{2}\sqrt{2}} + \frac{|01\rangle \langle 01|}{\sqrt{2}\sqrt{2}} \right) + \epsilon^2 \frac{|00\rangle \langle 00|}{\sqrt{2}\sqrt{2}} \quad (\text{S12})$$

$$= \frac{1}{2} (1-\epsilon) (|00\rangle \langle 11| + |11\rangle \langle 00|) + (\text{other terms unrelated to the } \hat{X} \otimes \hat{X} \text{ measurement}), \quad (\text{S13})$$

the expectation value is calculated as

$$\langle \hat{X} \otimes \hat{X} \otimes \hat{O} \rangle = (1-\epsilon) \langle \hat{X} \otimes \hat{X} \otimes \hat{O} \rangle_{\rho_{\text{Bell}}}. \quad (\text{S14})$$

Note that a similar calculation works for global amplitude damping noise. Therefore, when amplitude damping is dominant, we do not need twirling to make a Werner ancilla state.

C. A Bell state with local dephasing (T_2) noise

Next, we consider the case where the ideal Bell ancilla state suffers from local dephasing (T_2) noise described as $\mathcal{E}_{T_2}(\rho) = (1-\epsilon)\rho + \epsilon\hat{Z}\rho\hat{Z}$. Since the state is described as

$$(\mathcal{E}_{T_2} \otimes \mathcal{E}_{T_2})(\rho_{\text{Bell}}) = (1-\epsilon)^2 \rho_{\text{Bell}} + \epsilon(1-\epsilon)(\hat{Z} \otimes \hat{I})\rho_{\text{Bell}}(\hat{Z} \otimes \hat{I}) + \epsilon(1-\epsilon)(\hat{I} \otimes \hat{Z})\rho_{\text{Bell}}(\hat{I} \otimes \hat{Z}) + \epsilon^2(\hat{Z} \otimes \hat{Z})\rho_{\text{Bell}}(\hat{Z} \otimes \hat{Z}) \quad (\text{S15})$$

$$= \frac{(1-2\epsilon)^2}{2} (|00\rangle \langle 11| + |11\rangle \langle 00|) + (\text{other terms unrelated to the } \hat{X} \otimes \hat{X} \text{ measurement}), \quad (\text{S16})$$

the expectation value is calculated as

$$\langle \hat{X} \otimes \hat{X} \otimes \hat{O} \rangle = (1-2\epsilon)^2 \langle \hat{X} \otimes \hat{X} \otimes \hat{O} \rangle_{\rho_{\text{Bell}}}. \quad (\text{S17})$$

Therefore, when local dephasing (T_2) noise is dominant, we do not need twirling to make a Werner state.

S2. USING SEPARABLE ANCILLA STATE INSTEAD OF NOISY-ENTANGLEMENT ANCILLA STATE

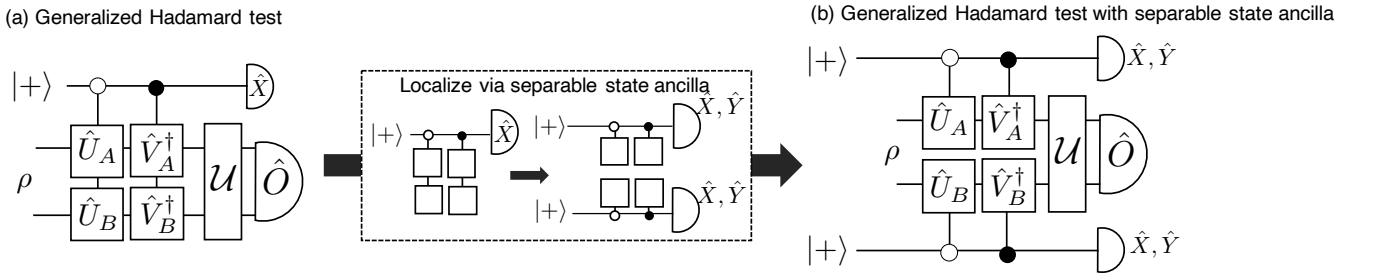


FIG. S2. (a) Generalized Hadamard test, which includes non-local controlled operations. (b) Generalized Hadamard test for DQC by replacing non-local controlled operations with the separable state ancilla, $|+\rangle \otimes |+\rangle$ and performing additional $\hat{Y} \otimes \hat{Y}$ measurements.

In the main text, we replace the non-local controlled operation with noisy entanglement ancilla and local controlled operations. Here, we show another replacement using separable state ancilla, $|+\rangle \otimes |+\rangle$ and additional $\hat{Y} \otimes \hat{Y}$ measurements as shown in Fig. S2. As shown below, this replacement doubles the sampling-cost factor $\gamma(n)$, leading to four-fold sampling overhead. Combining this replacement with ancilla reuse in the main text provides asymptotically optimal circuit knitting as shown in Fig. 1 in the main text. The calculation is similar to that for noisy entanglement above. Since the separable state ancilla is described as

$$\begin{aligned} |+\rangle \otimes |+\rangle &= \frac{1}{2}(|00\rangle \langle 11| + |11\rangle \langle 00| + |01\rangle \langle 10| + |10\rangle \langle 01|) \\ &+ (\text{other terms unrelated to the } \hat{X} \otimes \hat{X} \text{ and } \hat{Y} \otimes \hat{Y} \text{ measurements}), \end{aligned} \quad (\text{S18})$$

the expectation values of $\hat{X} \otimes \hat{X} \otimes \hat{O}$ and $\hat{Y} \otimes \hat{Y} \otimes \hat{O}$ are calculated as

$$\begin{aligned} &\langle \hat{X} \otimes \hat{X} \otimes \hat{O} \rangle \\ &= \frac{1}{4} \text{Tr}[\hat{O} \mathcal{U}((\hat{U}_A \otimes \hat{U}_B) \rho(\hat{V}_A \otimes \hat{V}_B) + (\hat{V}_A^\dagger \otimes \hat{U}_B) \rho(\hat{U}_A^\dagger \otimes \hat{V}_B) + (\hat{U}_A \otimes \hat{V}_B^\dagger) \rho(\hat{V}_A \otimes \hat{U}_B^\dagger) + (\hat{V}_A^\dagger \otimes \hat{V}_B^\dagger) \rho(\hat{U}_A^\dagger \otimes \hat{U}_B^\dagger))], \end{aligned} \quad (\text{S19})$$

$$\begin{aligned} &\langle \hat{Y} \otimes \hat{Y} \otimes \hat{O} \rangle \\ &= \frac{1}{4} \text{Tr}[\hat{O} \mathcal{U}(-(\hat{U}_A \otimes \hat{U}_B) \rho(\hat{V}_A \otimes \hat{V}_B) + (\hat{V}_A^\dagger \otimes \hat{U}_B) \rho(\hat{U}_A^\dagger \otimes \hat{V}_B) + (\hat{U}_A \otimes \hat{V}_B^\dagger) \rho(\hat{V}_A \otimes \hat{U}_B^\dagger) - (\hat{V}_A^\dagger \otimes \hat{V}_B^\dagger) \rho(\hat{U}_A^\dagger \otimes \hat{U}_B^\dagger))], \end{aligned} \quad (\text{S20})$$

respectively. From these expectation values, we have

$$\langle \hat{X} \otimes \hat{X} \otimes \hat{O} \rangle - \langle \hat{Y} \otimes \hat{Y} \otimes \hat{O} \rangle = \frac{1}{2} \text{Tr}[\hat{O} \mathcal{U}((\hat{U}_A \otimes \hat{U}_B) \rho(\hat{V}_A \otimes \hat{V}_B) + \text{h.c.})], \quad (\text{S21})$$

which is the same expectation value as that given by Eqs. (S1) and (S9). However, the additional measurement increases the variance of \hat{O} by a factor of four, quadruples the sampling overhead. This means that the additional measurement doubles $\gamma(n)$. A simple explanation of this is as follows. When we calculate $\langle \hat{X} \otimes \hat{X} \otimes \hat{O} \rangle - \langle \hat{Y} \otimes \hat{Y} \otimes \hat{O} \rangle$ by Monte-Carlo sampling, we may sample each term with a probability of 1/2, and thus we must double the sampling result, which increases its variance by a factor of four:

$$\text{Var} \left\{ 2 \times \left[\frac{1}{2} \langle \hat{X} \otimes \hat{X} \otimes \hat{O} \rangle + \frac{1}{2} (-\langle \hat{Y} \otimes \hat{Y} \otimes \hat{O} \rangle) \right] \right\} = 4 \text{Var}[\langle \hat{X} \otimes \hat{X} \otimes \hat{O} \rangle_{\rho_{\text{Bell}}}], \quad (\text{S22})$$

For a more general discussion of general observables, see Ref. [74].

S3. EFFECT OF NOISE IN THE PURIFICATION CIRCUIT

A. Details of numerical calculation

In the numerical calculation used to estimate the fidelity within local noise, we use the quantum circuits shown in Fig. S3, where we set $\hat{O} = \hat{P}_{\text{Bell}}$ for calculating the fidelity and $\rho_{\text{noisy}} = \rho_{\text{Werner}}$ for simplicity. Denoting the virtually purified state as ρ_{purified} , we obtain the purified fidelity to the Bell state as

$$\frac{\text{Tr}[(\hat{X} \otimes \hat{X} \otimes \hat{P}_{\text{Bell}})((\mathcal{E}_{\text{mes}} \otimes \mathcal{E}_{\text{mes}}) \circ \mathcal{V}_{\text{noisy}})(\rho_{\text{Werner}} \otimes \rho_{\text{noisy}})]}{\text{Tr}[(\hat{X} \otimes \hat{X} \otimes \hat{I})((\mathcal{E}_{\text{mes}} \otimes \mathcal{E}_{\text{mes}}) \circ \mathcal{V}_{\text{noisy}})(\rho_{\text{Werner}} \otimes \rho_{\text{noisy}})]} \equiv \frac{\text{Tr}[\hat{P}_{\text{Bell}} \rho_{\text{purified}}]}{\text{Tr}[\rho_{\text{purified}}]} = F_{\text{purified}}, \quad (\text{S23})$$

where $\mathcal{V}_{\text{noisy}}$ is the purification operation map including noise, shown as in Fig. S3; when there is no noise in the purification operations, $\rho_{\text{purified}} = \hat{P}_{\text{Bell}} \rho_{\text{noisy}} \hat{P}_{\text{Bell}}$ and $F_{\text{purified}} = 1$. In the numerical calculation, we use only six quantum circuits including control operation (shown as $\mathcal{V}_{2,\text{noisy}}$ in Fig. S3) instead of 12 quantum circuits because each circuit can sample two terms in $1/16 \sum_{i,j} \hat{S}_i \rho_{\text{noisy}} \hat{S}_j$ at once. For example, the quantum circuit at the top left within the dashed lines for $\mathcal{V}_{2,\text{noisy}}$ generates $1/2((\hat{X} \otimes \hat{X}) \rho_{\text{noisy}} (\hat{I} \otimes \hat{I}) + (\hat{I} \otimes \hat{I}) \rho_{\text{noisy}} (\hat{X} \otimes \hat{X}))$, so we can obtain two terms at once when we sample this quantum circuit with the probability of 1/8.

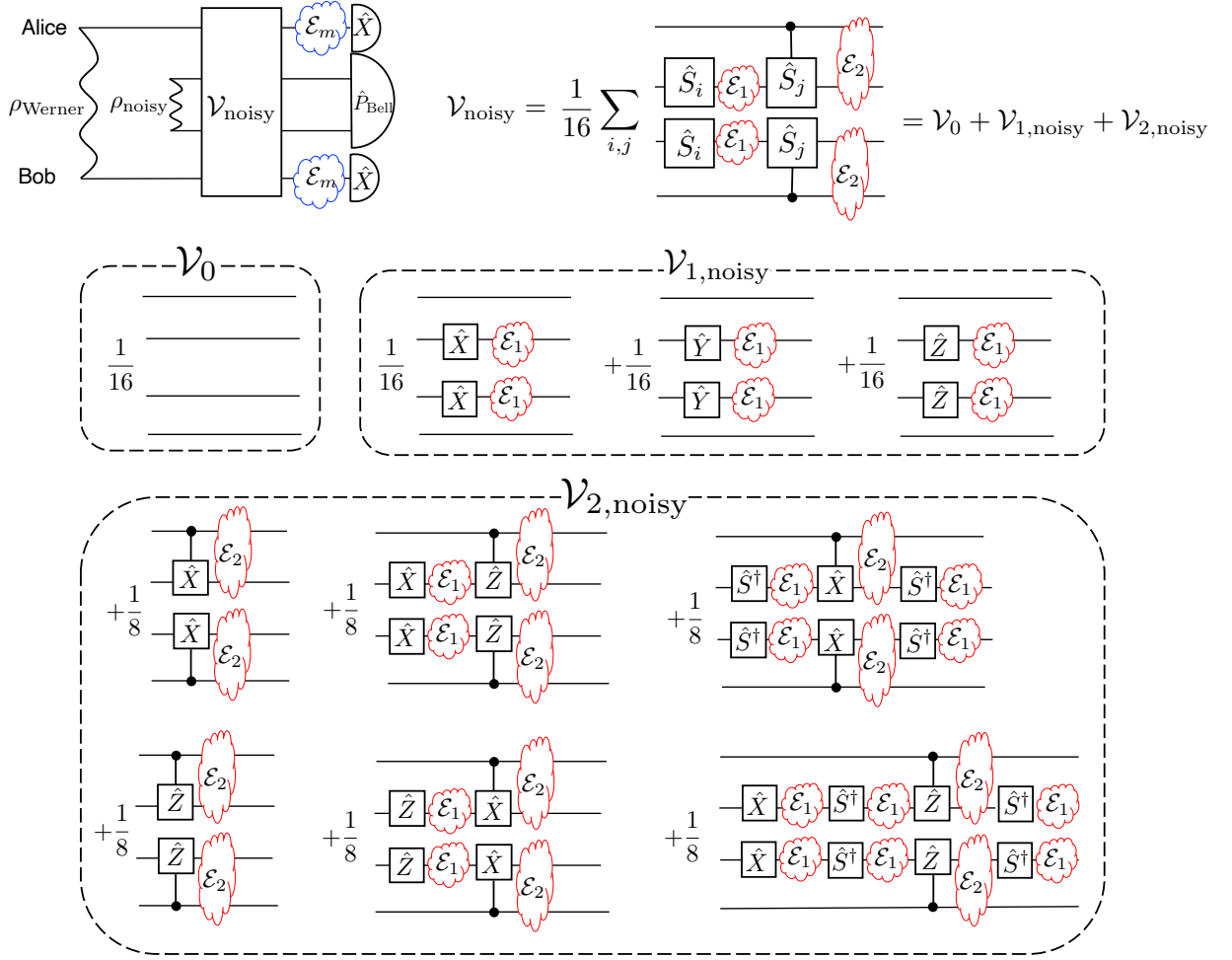


FIG. S3. Quantum circuits sampled for our numerical demonstration to calculate the fidelity, where we set $\rho_{\text{noisy}} = \rho_{\text{Werner}}$. Here, $\hat{P}_{\text{Bell}} = |\psi_{\text{Bell}}\rangle\langle\psi_{\text{Bell}}|$ denotes a Bell measurement. The purification operation map $\mathcal{V}_{\text{noisy}}$, including the noise in LOCC, is given by $\mathcal{V}_{\text{noisy}} = \mathcal{V}_0 + \mathcal{V}_{1,\text{noisy}} + \mathcal{V}_{2,\text{noisy}}$, where \mathcal{V}_0 is the identity map, $\mathcal{V}_{1,\text{noisy}}$ is the map including only single-qubit gates, and $\mathcal{V}_{2,\text{noisy}}$ the map including two-qubit gates. The error maps, $\mathcal{E}_1, \mathcal{E}_2, \mathcal{E}_{\text{mes}}$, describe local 1-qubit and 2-qubit noise map and measurement noise, respectively.

B. Analytical validation of the $\frac{8}{15}p_2\epsilon + (\text{higher-order terms})$ infidelity

We classify the purification operation $\mathcal{V}_{\text{noisy}}$ as $\mathcal{V}_{\text{noisy}} = \mathcal{V}_0 + \mathcal{V}_{1,\text{noisy}} + \mathcal{V}_{2,\text{noisy}}$, where \mathcal{V}_0 is the identity map, $\mathcal{V}_{1,\text{noisy}}$ is the map including only single-qubit gates, and $\mathcal{V}_{2,\text{noisy}}$ the map including two-qubit gates, because $\mathcal{E}_{\text{mes}}, \mathcal{E}_1$, and \mathcal{E}_2 affect differently on each map. Here,

$$\mathcal{E}_{\text{mes}}(\rho) = (1 - p_{\text{mes}})\rho + p_{\text{mes}}\hat{Z}\rho\hat{Z} \quad (\text{S24})$$

is the measurement noise,

$$\mathcal{E}_1(\rho) = (1 - p_1)\rho + \frac{p_1}{3} \sum_{\hat{P}=\hat{X},\hat{Y},\hat{Z}} \hat{P}\rho\hat{P} = \left(1 - \frac{4}{3}p_1\right)\rho + \frac{4}{3}p_1\frac{1}{4} \sum_{\hat{P}=\hat{I},\hat{X},\hat{Y},\hat{Z}} \hat{P}\rho\hat{P} \quad (\text{S25})$$

is the single-qubit noise, and

$$\mathcal{E}_2(\rho) = (1 - p_2)\rho + \frac{p_2}{15} \sum_{\hat{P}_1, \hat{P}_2=\hat{X},\hat{Y},\hat{Z}} (\hat{P}_1 \otimes \hat{P}_2)\rho(\hat{P}_1 \otimes \hat{P}_2) = \left(1 - \frac{16}{15}p_2\right)\rho + \frac{16}{15}p_2\frac{1}{16} \sum_{\hat{P}_1, \hat{P}_2=\hat{I},\hat{X},\hat{Y},\hat{Z}} (\hat{P}_1 \otimes \hat{P}_2)\rho(\hat{P}_1 \otimes \hat{P}_2) \quad (\text{S26})$$

is the 2-qubit noise.

Here, we analytically show that the infidelity becomes $\frac{8}{15}p_2\epsilon +$ (higher-order terms) by approximating $\mathcal{V}_{2,\text{noisy}} = (\mathcal{E}_2 \otimes \mathcal{E}_2) \circ \mathcal{V}_{2,\text{id}}$ for simplicity, where $\mathcal{V}_{2,\text{id}}$ is the purification operation including two-qubit gates without noise in the purification operations; see Fig. S4(a). In the following, \mathcal{V}_{id} and $\mathcal{V}_{1,\text{id}}$ are defined in the same way. We show Fig. S4(b) in advance to support the validity of these approximations in explaining the behavior of the p_2 dependence of fidelity.

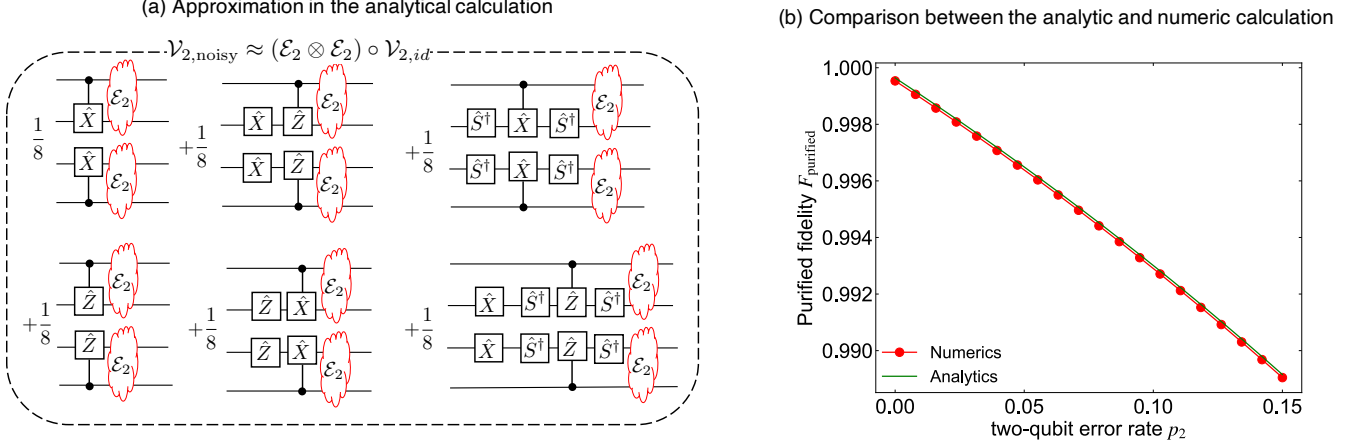


FIG. S4. (a) Schematic quantum circuits of the approximation used in the analytical calculation. (b) 2-qubit error-rate dependence of purified fidelity for numerical and analytical results in Eq. (S43). The correspondence shows that the analytic calculation with the approximation explains the numerical result well.

To calculate the fidelity in the presence of noise in the purification operation, we need to calculate

$$\text{Tr}[(\hat{X} \otimes \hat{X} \otimes \hat{O})((\mathcal{E}_{\text{mes}} \otimes \mathcal{E}_{\text{mes}}) \circ \mathcal{V}_{\text{noisy}})(\rho_{\text{Werner}} \otimes \rho_{\text{noisy}})] \quad (\text{S27})$$

for $\hat{O} = \hat{P}_{\text{Bell}}, \hat{I}$. For preparation, we first examine the effects of single-qubit and 2-qubit noise and measurement noise *in the expectation value*. Notably, as we show below, the 2-qubit noise and the measurement noise simply reduce the amplitude of the expectation value, which is different from the effects on a state itself. This is the essence of the low infidelity characteristics of our protocol.

First, for any operator \hat{O} and any state ρ , the measurement noise and the two-qubit noise reduce the amplitude of the trace only by a factor of $(1 - p_{\text{mes}})^2$ and $(1 - 16/p_2/15)^2$, respectively, as follows. For the measurement noise for any state ρ , we have

$$\text{Tr}[(\hat{X} \otimes \hat{X} \otimes \hat{O})(\mathcal{E}_{\text{mes}} \otimes \mathcal{E}_{\text{mes}})(\rho)] = \text{Tr}[(\mathcal{E}_{\text{mes}}(\hat{X}) \otimes \mathcal{E}_{\text{mes}}(\hat{X}) \otimes \hat{O})\rho] = (1 - 2p_{\text{mes}})^2 \text{Tr}[(\hat{X} \otimes \hat{X} \otimes \hat{O})\rho], \quad (\text{S28})$$

where we used

$$\mathcal{E}_{\text{mes}}(\hat{X}) = (1 - p_{\text{mes}})\hat{X} + p_{\text{mes}}\hat{Z}\hat{X}\hat{Z} = (1 - 2p_{\text{mes}})\hat{X}. \quad (\text{S29})$$

This calculation shows that the measurement noise reduces only the amplitude of the expectation value.

For the two-qubit noise for any states ρ , we have

$$\text{Tr}[(\hat{X} \otimes \hat{X} \otimes \hat{O})(\mathcal{E}_2 \otimes \mathcal{E}_2)(\rho)] = \text{Tr}[\rho(\mathcal{E}_2 \otimes \mathcal{E}_2)(\hat{X} \otimes \hat{X} \otimes \hat{O})] = \left(1 - \frac{16}{15}p_2\right)^2 \text{Tr}[(\hat{X} \otimes \hat{X} \otimes \hat{O})\rho], \quad (\text{S30})$$

where we used

$$\begin{aligned}
(\mathcal{E}_2 \otimes \mathcal{E}_2)(\hat{X} \otimes \hat{X} \otimes \hat{O}) &= \left(1 - \frac{16}{15}p_2\right)^2 \hat{X} \otimes \hat{X} \otimes \hat{O} \\
&+ \left(1 - \frac{16}{15}p_2\right) \left(\frac{16}{15}p_2\right) \frac{1}{16} \sum_{\hat{P}_1, \hat{P}_2 = \hat{I}, \hat{X}, \hat{Y}, \hat{Z}} \left[(\hat{P}_1 \hat{X} \hat{P}_1) \otimes \hat{X} \otimes [(\hat{P}_2 \otimes \hat{I})\hat{O}(\hat{P}_2 \otimes \hat{I})] + \hat{X} \otimes (\hat{P}_1 \hat{X} \hat{P}_1) \otimes [(\hat{I} \otimes \hat{P}_2)\hat{O}(\hat{I} \otimes \hat{P}_2)] \right] \\
&+ \left(\frac{16}{15}p_2\right)^2 \frac{1}{16^2} \sum_{\hat{P}_1, \hat{P}_2, \hat{P}_3, \hat{P}_4 = \hat{I}, \hat{X}, \hat{Y}, \hat{Z}} (\hat{P}_1 \hat{X} \hat{P}_1) \otimes (\hat{P}_2 \hat{X} \hat{P}_2) \otimes [(\hat{P}_3 \otimes \hat{P}_4)\hat{O}(\hat{P}_3 \otimes \hat{P}_4)] \\
&= \left(1 - \frac{16}{15}p_2\right)^2 \hat{X} \otimes \hat{X} \otimes \hat{O}.
\end{aligned} \tag{S31}$$

Here the terms in the second and third lines vanish because

$$\sum_{\hat{P}_1 = \hat{I}, \hat{X}, \hat{Y}, \hat{Z}} (\hat{P}_1 \hat{X} \hat{P}_1) \otimes \hat{X} = \sum_{\hat{P}_1 = \hat{I}, \hat{X}, \hat{Y}, \hat{Z}} \hat{X} \otimes (\hat{P}_1 \hat{X} \hat{P}_1) = \sum_{\hat{P}_1, \hat{P}_2 = \hat{I}, \hat{X}, \hat{Y}, \hat{Z}} (\hat{P}_1 \hat{X} \hat{P}_1) \otimes (\hat{P}_2 \hat{X} \hat{P}_2) = 0. \tag{S33}$$

Finally, we consider the single-qubit noise. For any state ρ , we have

$$\text{Tr}[\hat{X} \otimes \hat{X} \otimes \hat{O}(\mathcal{E}_1 \otimes \mathcal{E}_1)(\rho)] = \text{Tr}[(\hat{X} \otimes \hat{X} \otimes [(\mathcal{E}_1 \otimes \mathcal{E}_1)(\hat{O})])\rho] \tag{S34}$$

$$= \begin{cases} (1 - \frac{4}{3}p_1)^2 \text{Tr}[(\hat{X} \otimes \hat{X} \otimes \hat{P}_{\text{Bell}})\rho] + \frac{1}{4} \left[1 - (1 - \frac{4}{3}p_1)^2\right] \text{Tr}[(\hat{X} \otimes \hat{X} \otimes \hat{P}_{\text{Bell}})\rho] & \text{(for } \hat{O} = \hat{P}_{\text{Bell}}) \\ \text{Tr}[(\hat{X} \otimes \hat{X} \otimes \hat{P}_{\text{Bell}})\rho] & \text{(for } \hat{O} = \hat{I}) \end{cases}, \tag{S35}$$

where we used

$$\begin{aligned}
(\mathcal{E}_1 \otimes \mathcal{E}_1)(\hat{O}) &= \left(1 - \frac{4}{3}p_1\right)^2 \hat{O} + \left(1 - \frac{4}{3}p_1\right) \left(\frac{4}{3}p_1\right) \frac{1}{4} \sum_{\hat{P} = \hat{I}, \hat{X}, \hat{Y}, \hat{Z}} (\hat{P} \otimes \hat{I})\hat{O}(\hat{P} \otimes \hat{I}) + (\hat{I} \otimes \hat{P})\hat{O}(\hat{I} \otimes \hat{P}) \\
&+ \left(\frac{4}{3}p_1\right)^2 \frac{1}{16} \sum_{\hat{P}_1, \hat{P}_2 = \hat{I}, \hat{X}, \hat{Y}, \hat{Z}} (\hat{P}_1 \otimes \hat{P}_2)\hat{O}(\hat{P}_1 \otimes \hat{P}_2) \\
&= \begin{cases} \left(1 - \frac{4}{3}p_1\right)^2 \hat{O} + 2 \left(1 - \frac{4}{3}p_1\right) \left(\frac{4}{3}p_1\right) \frac{\hat{I}}{4} + \left(\frac{4}{3}p_1\right)^2 \frac{\hat{I}}{4} & \text{(for } \hat{O} = \hat{P}_{\text{Bell}}) \\ \hat{I} & \text{(for } \hat{O} = \hat{I}) \end{cases}
\end{aligned} \tag{S36}$$

$$= \begin{cases} \left(1 - \frac{4}{3}p_1\right)^2 \hat{O} + 2 \left(1 - \frac{4}{3}p_1\right) \left(\frac{4}{3}p_1\right) \frac{\hat{I}}{4} + \left(\frac{4}{3}p_1\right)^2 \frac{\hat{I}}{4} & \text{(for } \hat{O} = \hat{P}_{\text{Bell}}) \\ \hat{I} & \text{(for } \hat{O} = \hat{I}) \end{cases} \tag{S37}$$

The purified fidelity in Eq. (S23) is calculated as

$$F_{\text{purified}} = \frac{\text{Tr}[(\hat{X} \otimes \hat{X} \otimes \hat{P}_{\text{Bell}})[(\mathcal{E}_{\text{mes}} \otimes \mathcal{E}_{\text{mes}}) \circ \mathcal{V}_{\text{noisy}}(\rho_{\text{Werner}} \otimes \rho_{\text{noisy}})]]}{\text{Tr}[(\hat{X} \otimes \hat{X} \otimes \hat{I})[(\mathcal{E}_{\text{mes}} \otimes \mathcal{E}_{\text{mes}}) \circ \mathcal{V}_{\text{noisy}}(\rho_{\text{Werner}} \otimes \rho_{\text{noisy}})]]} \tag{S38}$$

$$= \frac{(1 - 2p_{\text{mes}})^2 \text{Tr}[(\hat{X} \otimes \hat{X} \otimes \hat{P}_{\text{Bell}})[(\mathcal{V}_0 + \mathcal{V}_{1,\text{noisy}} + \mathcal{V}_{2,\text{noisy}})(\rho_{\text{Werner}} \otimes \rho_{\text{noisy}})]]}{(1 - 2p_{\text{mes}})^2 \text{Tr}[(\hat{X} \otimes \hat{X} \otimes \hat{I})[(\mathcal{V}_0 + \mathcal{V}_{1,\text{noisy}} + \mathcal{V}_{2,\text{noisy}})(\rho_{\text{Werner}} \otimes \rho_{\text{noisy}})]]} \tag{S39}$$

$$\approx \frac{\text{Tr}[(\hat{X} \otimes \hat{X} \otimes \hat{P}_{\text{Bell}})[(\mathcal{V}_0 + (\mathcal{E}_1 \otimes \mathcal{E}_1) \circ \mathcal{V}_{1,\text{id}} + (\mathcal{E}_2 \otimes \mathcal{E}_2) \circ \mathcal{V}_{2,\text{id}})(\rho_{\text{Werner}} \otimes \rho_{\text{noisy}})]]}{\text{Tr}[(\hat{X} \otimes \hat{X} \otimes \hat{I})[(\mathcal{V}_0 + (\mathcal{E}_1 \otimes \mathcal{E}_1) \circ \mathcal{V}_{1,\text{id}} + (\mathcal{E}_2 \otimes \mathcal{E}_2) \circ \mathcal{V}_{2,\text{id}})(\rho_{\text{Werner}} \otimes \rho_{\text{noisy}})]]}, \tag{S40}$$

where we used the approximation, $\mathcal{V}_{2,\text{noisy}} \approx (\mathcal{E}_2 \otimes \mathcal{E}_2) \circ \mathcal{V}_{2,\text{id}}$, in the last line; see also Fig. S4(a) for this approximation. By using $\mathcal{V}_0(\rho_{\text{Werner}} \otimes \rho_{\text{noisy}}) \equiv \rho_{0,\text{id}}$, $\mathcal{V}_{1,\text{id}}(\rho_{\text{Werner}} \otimes \rho_{\text{noisy}}) \equiv \rho_{1,\text{id}}$, and $\mathcal{V}_{2,\text{id}}(\rho_{\text{Werner}} \otimes \rho_{\text{noisy}}) \equiv \rho_{2,\text{id}}$ as a shorthand

notation, and by using Eqs. (S28), (S30), and (S37), we continue the calculation as below:

$$F_{\text{purified}} = \frac{\text{Tr} \left[(\hat{X} \otimes \hat{X} \otimes \hat{P}_{\text{Bell}}) \left(\rho_{0,\text{id}} + \left(1 - \frac{4}{3}p_1\right)^2 \rho_{1,\text{id}} + \left(1 - \frac{16}{15}p_2\right)^2 \rho_{2,\text{id}} \right) \right] + \frac{1}{4} \left[1 - \left(1 - \frac{4}{3}p_1\right)^2 \right] \text{Tr}[(\hat{X} \otimes \hat{X} \otimes \hat{I})\rho_{1,\text{id}}]}{\text{Tr} \left[(\hat{X} \otimes \hat{X} \otimes \hat{I}) \left(\rho_{0,\text{id}} + \rho_{1,\text{id}} + \left(1 - \frac{16}{15}p_2\right)^2 \rho_{2,\text{id}} \right) \right]}$$
(S41)

$$= \frac{1 - \epsilon + \frac{9}{64} \left[1 - \left(1 - \frac{4}{3}p_1\right)^2 \right] \left(1 - \frac{4}{3}\epsilon\right) - \frac{3}{4} \left[1 - \left(1 - \frac{16}{15}p_2\right)^2 \right] (1 - \epsilon)}{1 - \epsilon - \frac{3}{4} \left[1 - \left(1 - \frac{16}{15}p_2\right)^2 \right] \left(1 - \frac{4}{3}\epsilon\right)}$$
(S42)

$$= 1 - \frac{1}{4} \frac{\frac{9}{16} \left[1 - \left(1 - \frac{4}{3}p_1\right)^2 \right] \left(1 - \frac{4}{3}\epsilon\right) + \left[1 - \left(1 - \frac{16}{15}p_2\right)^2 \right] \epsilon}{1 - \epsilon - \frac{3}{4} \left[1 - \left(1 - \frac{16}{15}p_2\right)^2 \right] \left(1 - \frac{4}{3}\epsilon\right)}$$
(S43)

$$= 1 - \left(\frac{3}{8}p_1 + \frac{8}{15}p_2\epsilon + (\text{higher-order terms}) \right).$$
(S44)

Here, ϵ is the initial infidelity of the noisy Bell state. Therefore, the infidelity after our protocol is $\frac{3}{8}p_1 + \frac{8}{15}p_2\epsilon +$ (higher-order terms). The first to the second lines use the following calculations:

$$\text{Tr}[(\hat{X} \otimes \hat{X} \otimes \hat{P}_{\text{Bell}})(\rho_{0,\text{id}} + \rho_{1,\text{id}} + \rho_{2,\text{id}})] = \text{Tr}[\hat{P}_{\text{Bell}}(\hat{P}_{\text{Bell}}\rho_{\text{noisy}}\hat{P}_{\text{Bell}})] = 1 - \epsilon,$$
(S45)

$$\text{Tr}[(\hat{X} \otimes \hat{X} \otimes \hat{I})(\rho_{0,\text{id}} + \rho_{1,\text{id}} + \rho_{2,\text{id}})] = \text{Tr}[\hat{P}_{\text{Bell}}\rho_{\text{noisy}}\hat{P}_{\text{Bell}}] = 1 - \epsilon,$$
(S46)

$$\text{Tr}[(\hat{X} \otimes \hat{X} \otimes \hat{P}_{\text{Bell}})\rho_{0,\text{id}}] = \frac{1}{16} \text{Tr} \left[\hat{P}_{\text{Bell}}[(\hat{I} \otimes \hat{I})\rho_{\text{noisy}}(\hat{I} \otimes \hat{I})] \right] = \frac{1}{16} \text{Tr}[\hat{P}_{\text{Bell}}\rho_{\text{noisy}}] = \frac{1}{16}(1 - \epsilon),$$
(S47)

$$\text{Tr}[(\hat{X} \otimes \hat{X} \otimes \hat{I})\rho_{0,\text{id}}] = \frac{1}{16} \text{Tr} \left[(\hat{I} \otimes \hat{I})\rho_{\text{noisy}}(\hat{I} \otimes \hat{I}) \right] = \frac{1}{16} \text{Tr}[\rho_{\text{noisy}}] = \frac{1}{16},$$
(S48)

$$\text{Tr}[(\hat{X} \otimes \hat{X} \otimes \hat{P}_{\text{Bell}})\rho_{1,\text{id}}] = \frac{1}{16} \text{Tr} \left[\hat{P}_{\text{Bell}} \sum_{\hat{P}=\hat{X},\hat{Y},\hat{Z}} (\hat{P} \otimes \hat{P})\rho_{\text{noisy}}(\hat{P} \otimes \hat{P}) \right] = \frac{3}{16} \text{Tr}[\hat{P}_{\text{Bell}}\rho_{\text{noisy}}] = \frac{3}{16}(1 - \epsilon),$$
(S49)

$$\text{Tr}[(\hat{X} \otimes \hat{X} \otimes \hat{I})\rho_{1,\text{id}}] = \frac{1}{16} \text{Tr} \left[\sum_{\hat{P}=\hat{X},\hat{Y},\hat{Z}} (\hat{P} \otimes \hat{P})\rho_{\text{noisy}}(\hat{P} \otimes \hat{P}) \right] = \frac{3}{16} \text{Tr}[\rho_{\text{noisy}}] = \frac{3}{16},$$
(S50)

$$\text{Tr}[(\hat{X} \otimes \hat{X} \otimes \rho_{\text{Bell}})\rho_{2,\text{id}}] = \text{Tr}[(\hat{X} \otimes \hat{X} \otimes \hat{P}_{\text{Bell}})(\rho_{0,\text{id}} + \rho_{1,\text{id}} + \rho_{2,\text{id}} - \rho_{0,\text{id}} - \rho_{1,\text{id}})] = \frac{3}{4}(1 - \epsilon),$$
(S51)

$$\text{Tr}[(\hat{X} \otimes \hat{X} \otimes \hat{I})\rho_{2,\text{id}}] = \text{Tr}[(\hat{X} \otimes \hat{X} \otimes \hat{I})(\rho_{0,\text{id}} + \rho_{1,\text{id}} + \rho_{2,\text{id}} - \rho_{0,\text{id}} - \rho_{1,\text{id}})] = (1 - \epsilon) - \frac{1}{4} = \frac{3}{4} - \epsilon.$$
(S52)

S4. ESTIMATION OF FIDELITY AND γ FOR REUSING THE WERNER STATE ANCILLA GIVEN $n = 1$ DATA

Here we analytically calculate the fidelity and the sampling-cost factor $\gamma(n)$ for reusing a Werner ancilla state (Fig. S5 (a)), based on the data for $n = 1$ with noisy purification operations. As shown in Fig. S7 later, we confirm the correspondence between this estimation and the numerical calculation for $n = 2, 3, 4$. To estimate the fidelity, yield, and $\gamma(n)$, we need to calculate

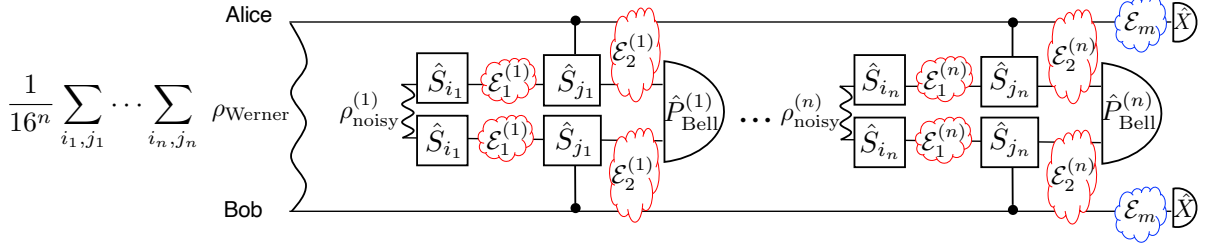
$$\text{Tr} \left[\left(\hat{X} \otimes \hat{X} \otimes \bigotimes_{\ell=1}^n \hat{O}^{(\ell)} \right) \left[\left(\mathcal{E}_{\text{mes}} \otimes \mathcal{E}_{\text{mes}} \right) \circ \mathcal{V}_{\text{noisy}}^{(n)} \circ \dots \circ \mathcal{V}_{\text{noisy}}^{(1)} \left(\rho_{\text{Werner}} \otimes \bigotimes_{\ell=1}^n \rho_{\text{noisy}}^{(\ell)} \right) \right] \right],$$
(S53)

where

$$\mathcal{V}_{\text{noisy}}^{(\ell)} \equiv \mathcal{V}_0^{(\ell)} + \mathcal{V}_{1,\text{noisy}}^{(\ell)} + \mathcal{V}_{2,\text{noisy}}^{(\ell)}$$
(S54)

are the noisy operations between the ancilla and ℓ -th noisy state, where $\mathcal{V}_0^{(\ell)}$ is the identity map, $\mathcal{V}_{1,\text{noisy}}^{(\ell)}$ is the map including only single-qubit gate, and $\mathcal{V}_{2,\text{noisy}}^{(\ell)}$ is the map including a two-qubit controlled gate as shown in Fig. S5: see also Fig. S3.

(a) Quantum circuit with reusing the Werner state ancilla in the presence of noise in purification operations

(b) ℓ -th purification operation in the presence of noise

$$\mathcal{V}_{\text{noisy}}^{(\ell)} = \frac{1}{16} \sum_{i_\ell, j_\ell} \begin{array}{c} \text{---} \hat{S}_{i_\ell} \text{---} \mathcal{E}_1^{(\ell)} \text{---} \hat{S}_{j_\ell} \text{---} \mathcal{E}_2^{(\ell)} \text{---} \\ \text{---} \hat{S}_{i_\ell} \text{---} \mathcal{E}_1^{(\ell)} \text{---} \hat{S}_{j_\ell} \text{---} \mathcal{E}_2^{(\ell)} \text{---} \end{array} = \mathcal{V}_0^{(\ell)} + \mathcal{V}_{1,\text{noisy}}^{(\ell)} + \mathcal{V}_{2,\text{noisy}}^{(\ell)}$$

FIG. S5. (a) A quantum circuit to calculate the fidelity with ancilla reuse in the presence of noise. (b) The ℓ -th purification operation in the presence of noise.

A. Noiseless purification operations

Before considering noise in the purification operations, we review the calculation of the expectation value with the ancilla reuse without noise. As in the previous section, we denote the purification map without noise as \mathcal{V}_{id} . Denoting $\hat{O}^{(\ell)} = \hat{P}_{\text{Bell}}^{(\ell)} \hat{I}^{(\ell)}$ and $\mathcal{V}_{\text{id}}^{(\ell)}$ is the ℓ -th operation on the ancilla state and $\rho_{\text{noisy}}^{(\ell)}$ without noise as shown in Fig. S5, we have

$$\begin{aligned} & \text{Tr} \left[\left(\hat{X} \otimes \hat{X} \otimes \bigotimes_{\ell=1}^n \hat{O}^{(\ell)} \right) \left[\mathcal{V}_{\text{id}}^{(n)} \circ \dots \circ \mathcal{V}_{\text{id}}^{(1)} \left(\rho_{\text{Werner}} \otimes \bigotimes_{\ell=1}^n \rho_{\text{noisy}}^{(\ell)} \right) \right] \right] \\ &= \frac{1}{2} \left(1 - \frac{4}{3} \epsilon \right) \frac{1}{16^n} \sum_{i_1, j_1} \dots \sum_{i_n, j_n} \text{Tr} \left[\bigotimes_{\ell=1}^n \hat{O}^{(\ell)} \left[\left(\hat{S}_{i_\ell} \otimes \hat{S}_{i_\ell} \right) \rho_{\text{noisy}}^{(\ell)} \left(\hat{S}_{i_\ell} \hat{S}_{j_\ell} \otimes \hat{S}_{i_\ell} \hat{S}_{j_\ell} \right) + \text{h.c.} \right] \right] \end{aligned} \quad (\text{S55})$$

$$\equiv \frac{1}{2} \left(1 - \frac{4}{3} \epsilon \right) \frac{1}{16^n} \sum_{i_1, k_1} \dots \sum_{i_n, k_n} \text{Tr} \left[\bigotimes_{\ell=1}^n \hat{O}^{(\ell)} \left[\left(\hat{S}_{i_\ell} \otimes \hat{S}_{i_\ell} \right) \rho_{\text{noisy}}^{(\ell)} \left(\hat{S}_{k_\ell} \otimes \hat{S}_{k_\ell} \right) + \text{h.c.} \right] \right] \quad (\text{S56})$$

$$\begin{aligned} &= \frac{1}{2} \left(1 - \frac{4}{3} \epsilon \right) \text{Tr} \left[\bigotimes_{\ell=1}^n \hat{O}^{(\ell)} \left[\left(\frac{1}{4} \sum_{j_\ell=1}^4 \hat{S}_{i_\ell} \otimes \hat{S}_{i_\ell} \right) \rho_{\text{noisy}}^{(\ell)} \left(\frac{1}{4} \sum_{k_\ell=1}^4 \hat{S}_{k_\ell} \otimes \hat{S}_{k_\ell} \right) + \text{h.c.} \right] \right] \\ &= \left(1 - \frac{4}{3} \epsilon \right) \prod_{\ell=1}^n \text{Tr} \left[\hat{O}^{(\ell)} \hat{P}_{\text{Bell}}^{(\ell)} \rho_{\text{noisy}}^{(\ell)} \hat{P}_{\text{Bell}}^{(\ell)} \right], \end{aligned} \quad (\text{S57})$$

where we defined $\hat{S}_{k_\ell} \otimes \hat{S}_{k_\ell} \equiv \hat{S}_{i_\ell} \hat{S}_{j_\ell} \otimes \hat{S}_{i_\ell} \hat{S}_{j_\ell} \in \mathbb{S}$. We can obtain the expectation value as

$$\frac{\left(1 - \frac{4}{3} \epsilon \right) \prod_{\ell=1}^n \text{Tr} \left[\hat{O}^{(\ell)} \hat{P}_{\text{Bell}}^{(\ell)} \rho_{\text{noisy}}^{(\ell)} \hat{P}_{\text{Bell}}^{(\ell)} \right]}{\left(1 - \frac{4}{3} \epsilon \right) \prod_{\ell=1}^n \text{Tr} \left[\hat{P}_{\text{Bell}}^{(\ell)} \rho_{\text{noisy}}^{(\ell)} \hat{P}_{\text{Bell}}^{(\ell)} \right]} = \prod_{\ell=1}^n \text{Tr} [\hat{O}^{(\ell)} \rho_{\text{Bell}}]. \quad (\text{S58})$$

Note that setting $\hat{O} = \hat{P}_{\text{Bell}}$ gives the fidelity of n noisy states to the ideal Bell state, which is unity if the purification operations are noise free. The sampling cost is proportional to the inverse of the denominator, as

$$\gamma(n) = \left(1 - \frac{4}{3} \epsilon \right)^{-1} \text{Tr} \left[\bigotimes_{\ell=1}^n \hat{P}_{\text{Bell}}^{(\ell)} \rho_{\text{noisy}}^{(\ell)} \hat{P}_{\text{Bell}}^{(\ell)} \right]^{-1} \equiv \left(1 - \frac{4}{3} \epsilon \right)^{-1} \prod_{\ell=1}^n (F_{\text{noisy}}^{(\ell)})^{-1}, \quad (\text{S59})$$

where $F_{\text{noisy}}^{(\ell)}$ is the fidelity for ℓ -th noisy state.

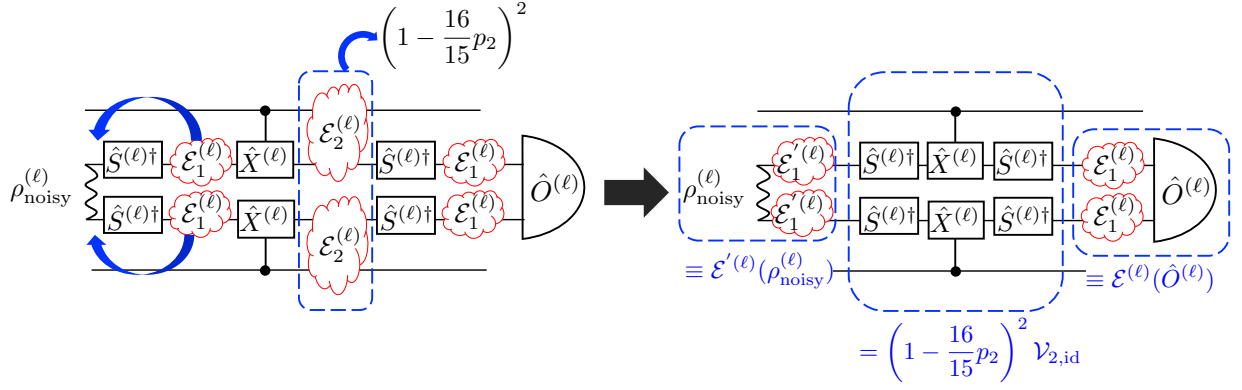


FIG. S6. Schematic illustration of the attribution of noise to the ℓ -th noisy state and ℓ -th measurement, taking one of the quantum circuits in $\mathcal{V}_{2,\text{noisy}}^{(\ell)}$ as an example.

B. Noisy LOCC

With noise in LOCC for ancilla reuse, we need numerical calculations to obtain the fidelity, yield, and $\gamma(n)$; this is problematic for large n due to the heavy numerical calculation loads. We avoid this by using $n = 1$ data as follows. The essential point to proceed with the calculation is that the two-qubit noise $\mathcal{E}_2^{(\ell)}$ in $\mathcal{V}_{2,\text{noisy}}^{(\ell)}$ simply reduces the amplitude of the trace as in Eq. (S30) as

$$\text{Tr} \left[\left(\hat{X} \otimes \hat{X} \otimes \bigotimes_{\ell=1}^n \hat{O}^{(\ell)} \right) [(\mathcal{E}_2 \otimes \mathcal{E}_2)(\rho)] \right] = \left(1 - \frac{16}{15} p_2 \right)^2 \text{Tr} \left[\left(\hat{X} \otimes \hat{X} \otimes \bigotimes_{\ell=1}^n \hat{O}^{(\ell)} \right) \rho \right], \quad (\text{S60})$$

and thus the noise in $\mathcal{V}_{2,\text{noisy}}^{(\ell)}$ in the trace can be considered to affect only on the ℓ -th noisy state and $\hat{O}^{(\ell)}$ as $(\mathcal{E}'_1^{(\ell)} \otimes \mathcal{E}_1^{(\ell)}) \circ \mathcal{V}_{2,\text{id}}^{(\ell)} \circ (\mathcal{E}_1^{(\ell)} \otimes \mathcal{E}'_1^{(\ell)})$, where $\mathcal{E}'_1^{(\ell)}$ and $\mathcal{E}_1^{(\ell)}$ are single-qubit noise maps deformed by the single-qubit gate included in $\mathcal{V}_{2,\text{id}}^{(\ell)}$ (see Fig. S6). Then all the noise in $\mathcal{V}_{\text{noisy}}^{(\ell)}$ can be attributed to the ℓ -th noisy state $\rho_{\text{noisy}}^{(\ell)}$ and the ℓ -th measurement $\hat{O}^{(\ell)}$, thereby decomposing the trace as follows.

$$\text{Tr} \left[\left(\hat{X} \otimes \hat{X} \otimes \bigotimes_{\ell=1}^n \hat{O}^{(\ell)} \right) \left[(\mathcal{E}_{\text{mes}} \otimes \mathcal{E}_{\text{mes}}) \circ \mathcal{V}_{\text{noisy}}^{(n)} \circ \dots \circ \mathcal{V}_{\text{noisy}}^{(1)} \left(\rho_{\text{Werner}} \otimes \bigotimes_{\ell=1}^n \rho_{\text{noisy}}^{(\ell)} \right) \right] \right] \quad (\text{S61})$$

$$= (1 - 2p_{\text{mes}})^2 \text{Tr} \left[\left(\hat{X} \otimes \hat{X} \otimes \bigotimes_{\ell=1}^n \hat{O}^{(\ell)} \right) \left[\mathcal{V}_{\text{noisy}}^{(n)} \circ \dots \circ \mathcal{V}_{\text{noisy}}^{(1)} \left(\rho_{\text{Werner}} \otimes \bigotimes_{\ell=1}^n \rho_{\text{noisy}}^{(\ell)} \right) \right] \right] \quad (\text{S62})$$

$$= (1 - 2p_{\text{mes}})^2 \text{Tr} \left[\left(\hat{X} \otimes \hat{X} \otimes \bigotimes_{\ell=1}^n \mathcal{E}^{(\ell)}(\hat{O}^{(\ell)}) \right) \left[\mathcal{V}_{\text{id}}^{(n)} \circ \dots \circ \mathcal{V}_{\text{id}}^{(1)} \left(\rho_{\text{Werner}} \otimes \bigotimes_{\ell=1}^n \mathcal{E}'^{(\ell)}(\rho_{\text{noisy}}^{(\ell)}) \right) \right] \right] \quad (\text{S63})$$

$$= (1 - 2p_{\text{mes}})^2 \left(1 - \frac{4}{3} \epsilon \right) \prod_{\ell=1}^n \text{Tr} \left[[\mathcal{E}^{(\ell)}(\hat{O}^{(\ell)})] \hat{P}_{\text{Bell}} [\mathcal{E}'^{(\ell)}(\rho_{\text{noisy}}^{(\ell)})] \hat{P}_{\text{Bell}} \right]. \quad (\text{S64})$$

Here, we define $\mathcal{E}^{(\ell)}$ and $\mathcal{E}'^{(\ell)}$ as the single-qubit noise including the effect of $\mathcal{E}_1^{(\ell)}$ and $\mathcal{E}'_1^{(\ell)}$, respectively (see Fig. S6).

In the numerical setting, we consider the same condition for all ℓ , that is,

$$\mathcal{E}^{(1)} = \mathcal{E}^{(2)} = \dots = \mathcal{E}^{(n)}, \quad \mathcal{E}'^{(1)} = \mathcal{E}'^{(2)} = \dots = \mathcal{E}'^{(n)}, \quad (\text{S65})$$

$$\rho_{\text{noisy}}^{(1)} = \rho_{\text{noisy}}^{(2)} = \dots = \rho_{\text{noisy}}^{(n)} = \rho_{\text{Werner}}, \quad \hat{O}^{(1)} = \hat{O}^{(2)} = \dots = \hat{O}^{(n)} = \hat{P}_{\text{Bell}} \text{ or } \hat{I}. \quad (\text{S66})$$

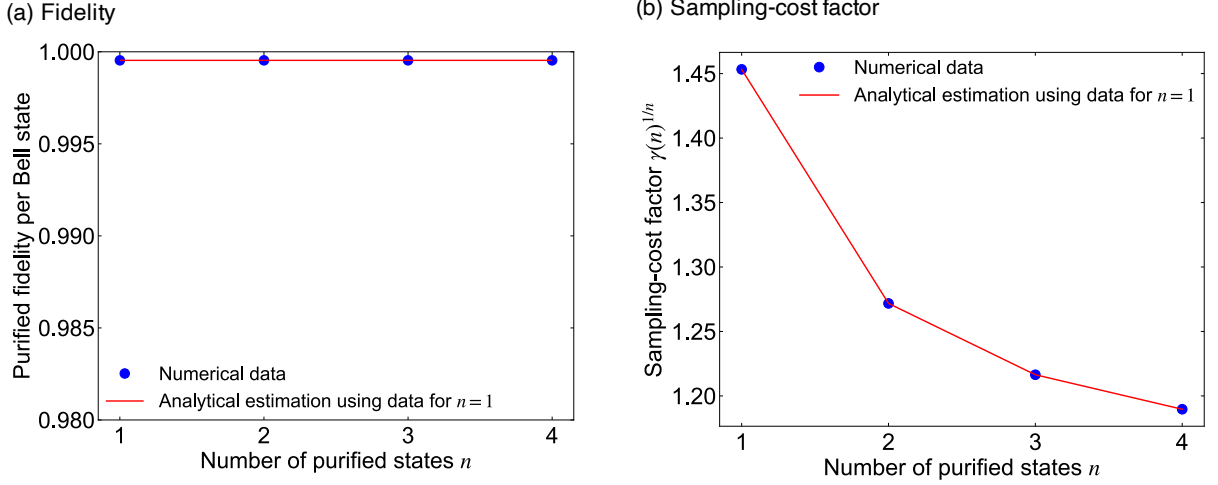


FIG. S7. Analytical estimation and numerical data for (a) fidelity and (b) sampling-cost factor per purified states n , $[\gamma(n)]^{1/n}$.

Therefore, from Eq. (S64), we have

$$(1 - 2p_{\text{mes}})^2 \left(1 - \frac{4}{3}\epsilon\right) \prod_{\ell=1}^n \text{Tr} \left[[\mathcal{E}^{(\ell)}(\hat{O}^{(\ell)})] \hat{P}_{\text{Bell}}[\mathcal{E}'^{(\ell)}(\rho_{\text{noisy}}^{(\ell)})] \hat{P}_{\text{Bell}} \right] \quad (\text{S67})$$

$$= (1 - 2p_{\text{mes}})^2 \left(1 - \frac{4}{3}\epsilon\right) \left(\text{Tr} \left[[\mathcal{E}^{(1)}(\hat{O}^{(1)})] \hat{P}_{\text{Bell}}[\mathcal{E}'^{(1)}(\rho_{\text{noisy}}^{(1)})] \hat{P}_{\text{Bell}} \right] \right)^n \quad (\text{S68})$$

$$= (1 - 2p_{\text{mes}})^{2-2n} \left(1 - \frac{4}{3}\epsilon\right)^{1-n} \cdot (\text{Data for } n=1)^n, \quad (\text{S69})$$

where

$$(\text{Data for } n=1) \equiv \text{Tr} \left[\left(\hat{X} \otimes \hat{X} \otimes \bigotimes_{\ell=1}^n \hat{O}^{(\ell)} \right) \left[(\mathcal{E}_{\text{mes}} \otimes \mathcal{E}_{\text{mes}}) \circ \mathcal{V}_{\text{noisy}}^{(1)} \left(\rho_{\text{Werner}} \otimes \rho_{\text{noisy}}^{(1)} \right) \right] \right] \quad (\text{S70})$$

$$= (1 - 2p_{\text{mes}})^2 \text{Tr} \left[\left(\hat{X} \otimes \hat{X} \otimes \mathcal{E}^{(1)}(\hat{O}^{(1)}) \right) \left[\mathcal{V}_{\text{id}}^{(1)} \left(\rho_{\text{Werner}} \otimes \mathcal{E}'^{(1)}(\rho_{\text{noisy}}^{(1)}) \right) \right] \right] \quad (\text{S71})$$

$$= (1 - 2p_{\text{mes}})^2 \left(1 - \frac{4}{3}\epsilon\right) \text{Tr} \left[[\mathcal{E}^{(1)}(\hat{O}^{(1)})] \hat{P}_{\text{Bell}}[\mathcal{E}'^{(1)}(\rho_{\text{noisy}}^{(1)})] \hat{P}_{\text{Bell}} \right] \quad (\text{S72})$$

can be obtained by the numerical simulation for $n=1$. This equation allows us to calculate the fidelity, yield, and $\gamma(n)$ for any n by using only the data for $n=1$.

Figure S7 shows this analytical estimation and numerical calculation for $n=2, 3, 4$. As we observe, this analytical estimation perfectly corresponds to the numerical calculation.

S5. PROBABILISTIC ERROR CANCELLATION (PEC) FOR BELL-STATE PREPARATION USING ONLY LOCC

PEC is one of the error mitigation methods [52, 70, 71], which effectively implements the inverse of the error map by post-processing at the cost of the number of sampling shots. Suppose the ideal noiseless state is ρ_{ideal} and the error map acting on the ideal state is \mathcal{E} . By decomposing the inverse of the error map as $\mathcal{E}^{-1} = \sum_i \eta_i \mathcal{B}_i$ with $\sum_i \eta_i = 1$, $\eta_i \in \mathbb{R}$, the error-mitigated state is described as $\rho_{\text{QEM}} = \mathcal{E}^{-1} \circ \mathcal{E}(\rho_{\text{ideal}}) = \sum_i \eta_i \mathcal{B}_i \mathcal{E}(\rho_{\text{ideal}})$. To simulate this decomposition with negative probability, we rewrite it as $\rho_{\text{QEM}} = \sum_i \eta_i \mathcal{B}_i \mathcal{E}(\rho_{\text{ideal}}) = \gamma \sum_i q_i \text{sgn}(\eta_i) \mathcal{B}_i \mathcal{E}(\rho_{\text{ideal}})$, where $\gamma = \sum_i |\eta_i| \geq 1$ is the sampling-cost factor and $q_i = |\eta_i|/\gamma$ is the sampling probability. The sampling shots that need to obtain the same accuracy without PEC scales with γ^2 [71].

Here we use PEC to suppress the error of a noisy Bell state. We consider a protocol for a Werner state without loss of generality since any bipartite noisy state can be transformed by appropriate twirling into a Werner state [60].

Although Ref. [54] recently showed the inverse map that satisfies the lower bound of the sampling cost for PEC, we provide a practical and concrete protocol by constructing the inverse map using only Pauli operations and by providing efficient estimation of the error rate.

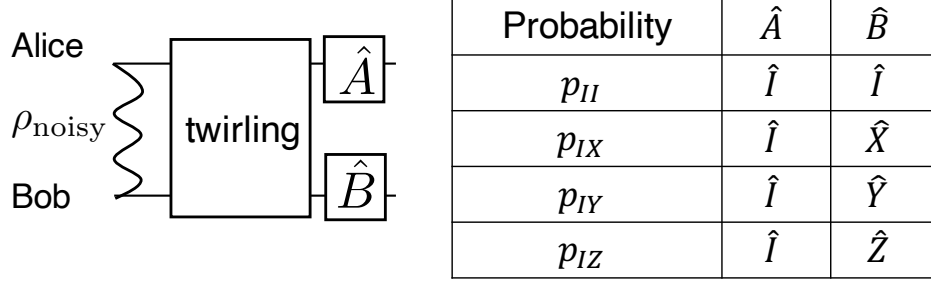


FIG. S8. Schematic illustration of probabilistic error cancellation (PEC) for a noisy Bell state ρ_{noisy} . In PEC, we insert $\hat{I} \otimes \hat{I}$ with probability p_{II} , $\hat{I} \otimes \hat{X}$ with p_{IX} , $\hat{I} \otimes \hat{Z}$ with p_{IY} , and $\hat{I} \otimes \hat{Z}$ with p_{IZ} , respectively, and then multiply the output of the last measurement by $\gamma \text{sgn}(\eta_i)$.

A. PEC for Bell-diagonal state

Here, we explain the application of PEC to the Bell-diagonal state as defined in Eq. (S3). Any bipartite noisy state can be transformed by appropriate twirling into a Bell-diagonal state [60]. After twirling, we need to estimate the error rates, $\epsilon_x, \epsilon_y, \epsilon_z$ (ϵ) for the Bell-diagonal (Werner) state. This could be done by standard tomography methods. Inspired by Ref. [72], here we describe below a more efficient method that uses a remote gate operation with the property of $(\mathcal{U}_\epsilon)^n = I$ for $n \equiv 0 \pmod{a}$, $a \in \mathbb{N}$; for example, we can use remote CNOT gates, i.e., $n \equiv 0 \pmod{2}$). We can estimate $\epsilon_x + \epsilon_y$ from the expected value obtained by preparing $|00\rangle$ state, applying non-local remote gates with noisy Bell states $n \equiv 0 \pmod{a}$ times, $(\mathcal{U}_\epsilon)^n$, and measuring the output on the $\{|00\rangle, |11\rangle\}$ basis. The expected value of the outcome is $\{1 + [1 - 2(\epsilon_x + \epsilon_y)]^n\}/2$. By doing the above procedure for different n and applying exponential fitting, we can estimate $\epsilon_x + \epsilon_y$. In particular, since $1/2$ at $n = 0$ is the fixed value, the simplest way is to do the above procedure for $n = 2$ and exponential fit these two points. Similarly, we can estimate $\epsilon_y + \epsilon_z$ by preparing $|++\rangle$ state, applying non-local remote gates with noisy Bell states $n \equiv 0 \pmod{a}$ times, and measuring the output on the $\{|--\rangle, |++\rangle\}$ basis, whose expectation value of outcome is $\{1 + [1 - 2(\epsilon_x + \epsilon_y)]^n\}/2$. Moreover, by preparing $|0+\rangle$ state, applying non-local remote gates with noisy Bell states $n \equiv 0 \pmod{a}$ times, and measuring the output in the $\{|0-\rangle, |1+\rangle\}$ basis, we can estimate the expectation value of the outcome as $\{1 + [1 - 2(\epsilon_x + \epsilon_y)]^n + [1 - 2(\epsilon_y + \epsilon_z)]^n + [1 - 2(\epsilon_x + \epsilon_z)]^n\}/4$. Note that, for a Werner state, we only have to do one estimation of the three kinds of estimation above since $\epsilon_x = \epsilon_y = \epsilon_z$.

Once we estimate the error rate, $\epsilon_x, \epsilon_y, \epsilon_z$, we can apply the inverse map as follows:

$$\mathcal{E}^{-1}(\rho_{\text{diag}}) = q_{II}\rho_{\text{diag}} + q_{IX}(\hat{I} \otimes \hat{X})\rho(\hat{I} \otimes \hat{X}) + q_{IY}(\hat{I} \otimes \hat{Y})\rho_{\text{diag}}(\hat{I} \otimes \hat{Y}) + q_{IZ}(\hat{I} \otimes \hat{Z})\rho_{\text{diag}}(\hat{I} \otimes \hat{Z}), \quad (\text{S73})$$

where

$$q_{II} = \frac{1}{4} \left(1 + \frac{1}{1 - 2(\epsilon_y + \epsilon_z)} + \frac{1}{1 - 2(\epsilon_x + \epsilon_z)} + \frac{1}{1 - 2(\epsilon_x + \epsilon_y)} \right), \quad (\text{S74})$$

$$q_{IX} = \frac{1}{4} \left(1 + \frac{1}{1 - 2(\epsilon_y + \epsilon_z)} - \frac{1}{1 - 2(\epsilon_x + \epsilon_z)} - \frac{1}{1 - 2(\epsilon_x + \epsilon_y)} \right), \quad (\text{S75})$$

$$q_{IY} = \frac{1}{4} \left(1 - \frac{1}{1 - 2(\epsilon_y + \epsilon_z)} + \frac{1}{1 - 2(\epsilon_x + \epsilon_z)} - \frac{1}{1 - 2(\epsilon_x + \epsilon_y)} \right), \quad (\text{S76})$$

$$q_{IZ} = \frac{1}{4} \left(1 - \frac{1}{1 - 2(\epsilon_y + \epsilon_z)} - \frac{1}{1 - 2(\epsilon_x + \epsilon_z)} - \frac{1}{1 - 2(\epsilon_x + \epsilon_y)} \right). \quad (\text{S77})$$

The sampling overhead is

$$\gamma = q_{II} + |q_{IX}| + |q_{IY}| + |q_{IZ}|. \quad (\text{S78})$$

The derivation of these values is almost the same as for the PEC for stochastic Pauli error, which is explained in, for example, App. A in Ref. [73].

The whole protocol is as follows.

1. Alice and Bob share a noisy Bell state. The noise information has to be obtained anyway to decide q_i for $i \in \{II, IX, IY, IZ\}$.
2. Alice samples i with probability $p_i \equiv |q_i|/\gamma$ and tells i to Bob. Similarly to the procedure of VQED, a person who samples i can be Bob or another person.
3. Alice and Bob apply the corresponding operation to the shared noisy Bell state, $\hat{I} \otimes \hat{I}$ for $i = II$, $\hat{I} \otimes \hat{X}$ for $i = IX$, $\hat{I} \otimes \hat{Y}$ for $i = IY$, $\hat{I} \otimes \hat{Z}$ for $i = IZ$, respectively.
4. Run the whole quantum circuit, multiply the outcome by $\gamma \text{sgn}(\eta_i)$.
5. Average the outcome to obtain the desired expectation value.

B. PEC for a Werner state

For a Werner state, we require the error information for PEC, which can be obtained by various tomography methods. We show here a method inspired by Ref. [72], which uses a remote gate operation with a Werner state that has the property of $(\mathcal{U}_\epsilon)^n = I$ for $n \equiv 0 \pmod{a}$, $a \in \mathbb{N}$; for example, we can use remote CNOT gates so $n \equiv 0 \pmod{2}$. We can estimate ϵ from the expectation value obtained by preparing $|00\rangle$ state, applying non-local remote gates with noisy Bell states $n \equiv 0 \pmod{a}$ times, $(\mathcal{U}_\epsilon)^n$, and measuring the output on the $\{|00\rangle, |11\rangle\}$ basis. The expectation value of the outcome is $[1 + (1 - 4/3\epsilon)^n]/2$. The above procedure is repeated for different n and applying exponential fitting to estimates ϵ . In particular, since $1/2$ at $n = 0$ is a fixed value, the simplest approach is to perform the above procedure for $n = 2$ and apply an exponential fitting to these two points.

Once we estimate the error rate, we can apply the inverse map as

$$\mathcal{E}^{-1}(\rho_{\text{Werner}}) = q_{II}\rho_{\text{Werner}} + q_{IX}(\hat{I} \otimes \hat{X})\rho_{\text{Werner}}(\hat{I} \otimes \hat{X}) + q_{IY}(\hat{I} \otimes \hat{Y})\rho_{\text{Werner}}(\hat{I} \otimes \hat{Y}) + q_{IZ}(\hat{I} \otimes \hat{Z})\rho_{\text{Werner}}(\hat{I} \otimes \hat{Z}), \quad (\text{S79})$$

where $q_{II} = (3 - \epsilon)/(3 - 4\epsilon)$, $q_{IX} = q_{IY} = q_{IZ} = -\epsilon/(3 - 4\epsilon)$. The sampling overhead is

$$\gamma = q_{II} + |q_{IX}| + |q_{IY}| + |q_{IZ}| = 1 + \frac{6\epsilon}{3 - 4\epsilon}. \quad (\text{S80})$$

The whole protocol for Alice and Bob is as follows.

1. Alice and Bob share a noisy Bell state, twirl it into a Werner state, and obtain its noise information to decide q_i for $i \in \{II, IX, IY, IZ\}$.
2. They sample and share i with probability $p_i \equiv |q_i|/\gamma$.
3. They apply the corresponding operation to the shared noisy Bell state, $\hat{I} \otimes \hat{I}$ for $i = II$, $\hat{I} \otimes \hat{X}$ for $i = IX$, $\hat{I} \otimes \hat{Y}$ for $i = IY$, $\hat{I} \otimes \hat{Z}$ for $i = IZ$, respectively.
4. They run the whole quantum circuit, and multiply the outcome by $\gamma \text{sgn}(\eta_i)$.
5. They average the outcome to obtain the desired expectation value.